KEMENTERIAN SUMBER ASLI, ALAM SEKITAR
DAN PERUBAHAN IKLIM
Ministry of Natural Resources, Environment
and Climate Change

MALAYSIAN METEOROLOGICAL DEPARTMENT
MINISTRY OF NATURAL RESOURCES, ENVIRONMENT
AND CLIMATE CHANGE

Technical Note No. 5/2022

Weather Phenomenon Impacting the WRF Model Performance over Malaysia: Sensitivity of Precipitation Forecasts to Parameterizations Schemes used in MET Malaysia's Operational WRF Model

Muhammad Firdaus Ammar Bin Abdullah and
Muhammad Sofian Bin Muhammad Yusof

TECHNICAL NOTE NO. 5/2022

Weather Phenomenon Impacting the WRF Model Performance over Malaysia: Sensitivity of Precipitation Forecasts to Parameterizations Schemes used in MET Malaysia's Operational WRF Model

By
Muhammad Firdaus Ammar Bin Abdullah and
Muhammad Sofian Bin Muhammad Yusof

Perpustakaan Negara Malaysia Data Pengkatalogan-dalam-Penerbitan

Published and printed by:
Jabatan Meteorologi Malaysia
Jalan Sultan
46667 Petaling Jaya
Selangor Darul Ehsan
Malaysia

Contents

Weather Phenomenon Impacting the WRF Model Performance over Malaysia: Sensitivity of Precipitation Forecasts to Parameterizations Schemes used in MET Malaysia's Operational WRF Model

Muhammad Firdaus Ammar Bin Abdullah and
Muhammad Sofian Bin Muhammad Yusof

Research and Technical Development Division
Malaysian Meteorological Department

Abstract

Numerical Weather Prediction models contain numerous parameterizations for physical processes and numerical stability. Parameterizations are based on physical laws but typically contain parameters whose values are not known precisely. The values of the parameters directly or indirectly affect the performance of model, and thus uncertainties in parameter values may lead to sensitive results, especially with high resolution and sophisticated microphysics (e.g., Park and Droegemeier, 1999). Accordingly, optimal estimation of parameters is one of the essential factors in improving the accuracy of numerical forecasts. Precipitation forecasts in Malaysia (Peninsular Malaysia, Sabah and Sarawak) have always been a challenge due to the complexity of its orography and its location bordering the South China Sea and the Straits of Malacca. The seasonal march of the monsoons produce heavy rainfall events are frequent and 24-hour precipitation amounts exceeding 200 mm are reached every year. Despite being a small region (32,000 km^2), contrasts between precipitation amounts that are recorded in a particular event can be very large. To evaluate the sensitivity of precipitation forecasts to the cumulus parameterizations schemes used in the 3-km outer model domain and the impacts on the inner 1-km domain using explicit convective scheme was used to gauge the ability of the WRF model to simulate the most important features of rain events in Malaysia, several simulations for selected rain episodes have been performed.

1.0 Introduction

Malaysia located near the Equatorial Belt in the maritime continent is influenced by both the Southwest (SW) Monsoon from May to September and the Northeast (NE) Monsoon from November to March the following year. The mechanism during both monsoons is of different in nature whereby during the SW Monsoon the country experiences a drier weather period with occasional convective storms during the monsoon break and a wetter period due to the large-scale convergence characterized by the Cold Surges during the NE Monsoon. The inter-monsoon period is symbolized by afternoon rain and thunderstorms.

The abundance of moisture and heat in the tropics makes the environment the tropics conditionally instable triggering sudden convection. This makes it very difficult for Numerical Weather Prediction (NWP) Models in the tropics. The complexity of the local orography as well large-scale climate drivers in the tropics further complicates NWP over the Maritime Continent.

Key features, processes, and atmospheric phenomenon in the tropics such as the El-Nino Southern Oscillation (ENSO), Madden-Julian Oscillation (MJO), Equatorial Rossby Wave, Indian Ocean Dipole Mode, Cold Tongue Biases, march of the Intertropical Convergence Zones provide a profound impact on the weather regimes and patterns thus impacting model performance.

The Weather Research and Forecasting (WRF) Model from the National Centre for Atmospheric Research (NCAR) USA is impacted by the global models driving it which in turn are impacted ability of these models to pick-up the major synoptic scale features caused by the above mentioned major tropical features. This paper examines how the parameterization schemes effect the WRF Model forecast over Malaysia with emphasis on the cumulus parametrization schemes used in the model's 3-KM domain. The sensitivity of the parametrization schemes is crucial in understanding how the major weather patterns impact the model performance. The cases selected are primarily during the NE Monsoon as all the key features are present during this period. This is of course subject to the inter-annual variability and the intra-seasonal Oscillation. Much of operational weather and long-range (climate) forecasting has a

statistical basis. As a nonlinear dynamical system, the atmosphere is not perfectly predictable in a deterministic sense. Consequently, statistical methods are useful although dynamic downscaling of the atmosphere is crucial in understanding the physical nature of the atmosphere. Some statistical forecast methods operate without information from the fluid dynamical Numerical Weather Prediction (NWP) models. However, these NWP models have become the mainstay of weather forecasting for lead times ranging from one day to a week or so in advance.

Such pure statistical forecast methods are sometimes referred to as Classical, reflecting their prominence in the years before NWP information was available. These methods are still viable and useful at very short lead times (hours in advance), or very long lead times (weeks or more in advance), for which NWP information is not available with either sufficient promptness or accuracy, respectively.

Another important application of statistical methods to weather forecasting is in conjunction with NWP information. Statistical forecast equations routinely are used to post-process and enhance the results of dynamical forecasts at operational weather forecasting centers throughout the world and are essential as guidance products to aid weather forecasters. The combined statistical and dynamical approaches are especially important for providing forecasts for quantities and locations rather than grid points not represented by the NWP models. Thus, it is crucial to improve the dynamical process in weather models to substantiate the combination of data driven process with dynamically driven process.

2.0 Methodology

The WRF-ARW model version 4.2 with the non-hydrostatic switch was used to run the test cases. The model was run for the 0000UTC cycle for the forecast period 28 November to 1 December 2008, 4 to 7 December 2008 and 23 to 26 December 2008 for a 72-hour forecast range to gauge the precipitation forecasts performance and the sensitivity towards the parameterization settings based on the model configuration and simulation method as further described in the Section 3.0. The WRF Modeling System Program Components and operational procedure for these test runs are shown in **Figure 1**.

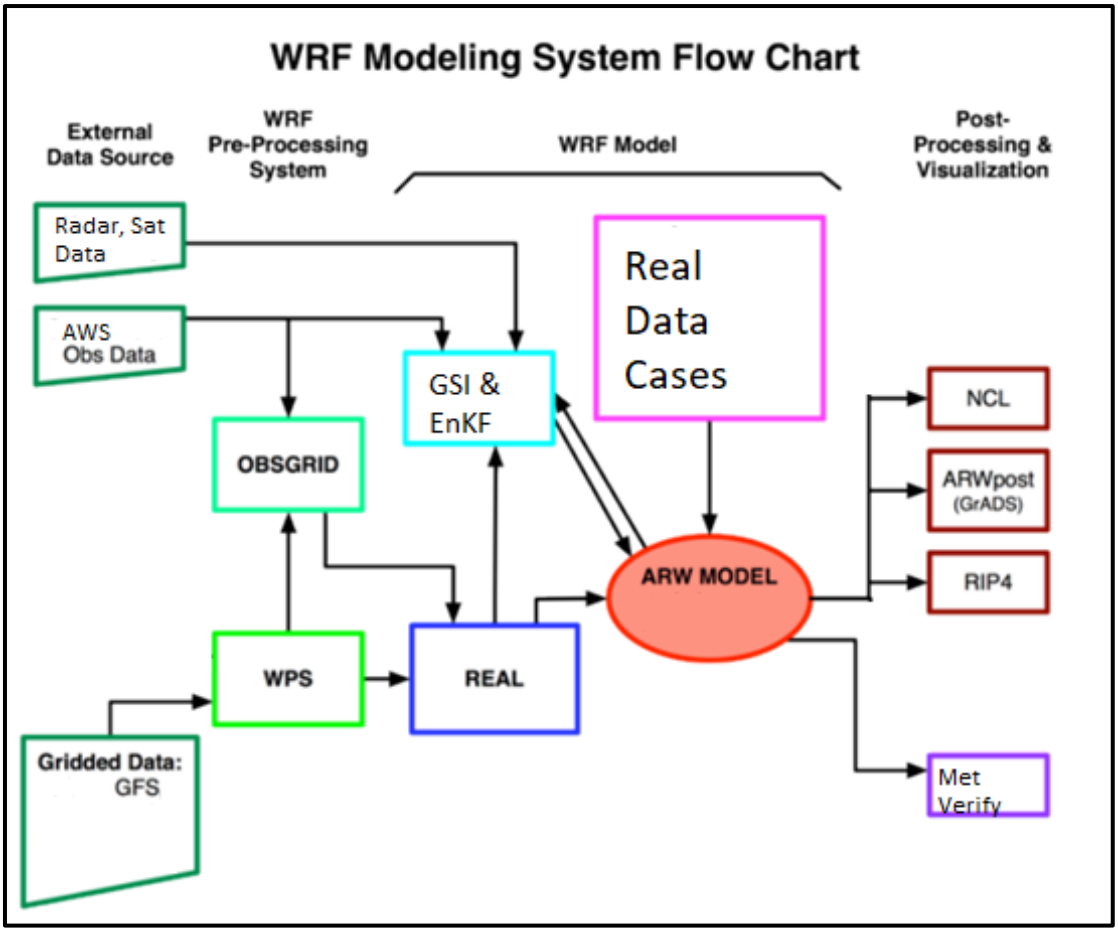

Figure 1: WRF Modelling Component Flowchart (National Centre for Atmospheric Research (NCAR) USA)

Based on **Figure 1**, as shown in the diagram, the WRF Modeling System consists of these major programs which is the WRF Preprocessing System (WPS), the assimilation system using Grid Point Statistical Interpolation (GSI) and Ensemble Kalman Filter, the ARW solver and the Post-processing & Visualization tool. In this research, we used ARWPOST utility from the WRF developers and The Grid Analysis and Display System (GrADS) for visualization purposes. Some post processing utilities from NCAR Graphics (NCL) and RIP4 were also used.

The ARW Solver used is the key component of the modeling system, which is composed of several initialization programs. We used real-data simulations and the numerical integration program. The key features of the WRF model simulations for these research include fully compressible nonhydrostatic equations , regional applications for the WRF Model, complete Coriolis and curvature terms, concurrent

one-way nesting with multiple nests and nest levels, , Mass-based hybrid sigma-pressure vertical coordinate, vertical grid-spacing varying with height, Map-scale factors using Mercator (conformal) projections , Arakawa C-grid staggering, Runge-Kutta 2nd and 3rd order time integration, Scalar-conserving flux form for prognostic variables , 2nd to 6th order advection (horizontal and vertical), Monotonic transport and positive-definite advection for moisture, scalar, tracer, and Turbulent Kinetic Energy , Time-split small step for acoustic and gravity-wave modes using external-mode filtering, Upper boundary absorption and Rayleigh damping, Lateral boundary conditions for real cases using full physics options for land-surface, planetary boundary layer, atmospheric and surface radiation, microphysics and cumulus convection, grid analysis nudging using separate upper-air and surface data, and observation Nudging, Adaptive time stepping, Orographic gravity wave drag. A detailed explanation of these options will not be given in this paper. However, the overall experimental design will be explained in Section 3.

Assessing the WRF Model performance and model sensitivity analysis was done using a dichotomous verification technique. The Met Malaysia's verification Package MET Verify developed in house was used. As we know, verification of weather forecasts has been undertaken since at least 1884 (Muller 1944; Murphy 1996). A wide variety of forecast verification procedures exist, but all involve measures of the relationship between a forecast or set of forecasts, and the corresponding observations of the predictand. Any forecast verification method involves comparisons between forecasts and the corresponding observations. The selected verification measure is a performance-based measure which focuses on the correspondence between forecast and observation either on an individual or collective basis (Murphy, 1997).

The validation of a model using observations can be cataloged into two general classes (Pielke (1974a)): -

(A) Subjective validation

One or more of the predicted fields are qualitatively compared against observations of a related phenomenon.

(B) **Point and pattern quantitative validation**

Point-to-point correspondence between model prediction and observation of the same meteorological parameter provides a quantitative test of model skill.

The evaluation method used to determine the forecast skill score is by calculating the Equitable threat score (ETS) and bias of the forecast. This score was developed by Gilbert in 1884 as a modification of the Critical Success Index to allow the number of hits that would have been obtained purely by chance. The ETS score is also known as the Gilbert Skill Score (GSS).

These scores are useful for evaluating non-probabilistic, gridded precipitation forecasts. ETS measures the fraction of observed and/or forecast events that were correctly predicted, adjusted for hits associated with random chance. Thus, making it easier to forecast rainfall accurately during the wet season compared to the dry season. ETS is often used in the verification of rainfall in NWP models because its "equitability" allows scores to be compared more fairly across different regimes. ETS is sensitive to hits because it penalizes both misses and false alarms in the same way, it does not distinguish the source of forecast error.

For a given precipitation threshold, forecasts are partitioned into a contingency table of four mutually exclusive and collectively exhaustive events: (*a*) the number of locations with both forecast and verification greater or equal than the threshold, that is, ‘‘hits;’’

(*b*) number of locations with forecast at or above the threshold and verification below, or ‘‘false alarms;’’ (*c*) number of locations with forecast below and verification at or above the threshold or ‘‘misses;’’ and (*d*) forecast and verification both below the threshold. We can summarize the above definition as follows:

i *hit* - event forecast to occur, and did occur
ii *miss* - event forecast not to occur, but did occur
iii *false alarm* - event forecast to occur, but did not occur

The performance of the forecast depends on the *yes events* of the forecast and the *yes events* of the observation. This is illustrated in **Table 1**.

Table 1: Contingency table of possible events

		Observed	
		YES	NO
Forecasts	YES	**a**	**b**
	NO	**c**	**d**

The **ETS** is defined by:

$ETS = (a-a_r)/(a+b+c-a_r)$ ----------(1)

a_r is the expected number of correct forecasts above the threshold in a random forecast, where forecast yes/no are independent of observation yeses/nos, defined by

$a_r = (a+b)(a+c)/(a+b+c+d)$----------(2)

The bias is the ratio of the number of yes forecasts issued divided by the number of yes observed:

$BIAS=(a+b)/(a+c)$----------(3)

The Range for ETS is from -1/3 to 1, where 0 indicates no skill and 1 indicates a perfect score. The range for the bias score is 0 to ∞**.** The bias score of 1 is categorized as perfect score. The methods for dichotomous (yes/no) forecasts are applied for verification of 24-h accumulated rainfall valid at 00 UTC every day. Both observed and forecast 24-h accumulated rainfalls are classified into five grades:

i. L: 0.1 – 9.9 mm/day
ii. M: 10 – 24.9 mm/day
iii. H: 25 – 49.9 mm/day
iv. S: 50 – 99.9 mm/day
v. T: >=100mm/day.

Although this method is not perfect and yields some inherent problems. The main problem with this validation technique is that spatial and temporal displacement of the

predicted from the observed fields could yield a poor verification. However so, this technique manages to answer two major questions: -

1. What fraction of the predicted convergence zones are covered by showers?

2. What fraction of the showers that occur lie inside of the predicted convergence zones?

3.0 WRF Model Configuration

3.1 Model Domains

Simulations were performed using the domain settings in **Figure 2**. One-way nesting was used in this experiment. The three nested domains are Domain 1, 9 KM resolution which covers the Southeast Asia region. Domain 2 has a 3-km which covers the whole Malaysian region. Domain 3 is at 1 KM resolution and covers Malaysia as well. There are 51 levels vertical levels.

The domains were carefully selected for numerical stability and to reduce the computing cost required for the test runs as this experiment were conducted on the operational High-Performance Computing (HPC) Cluster at MET Malaysia.

We introduced a sub-km (333 M) run within the 1 km using the nestdown approach to compare with the 1-KM runs to study the role of the urban canopy and the city scale Planetary Boundary Layer. However, this will not be discussed in this research publication. The 9-KM Domain has 368 x 368 grid points, the 3-km Domain has 886 x 442 grid points, and the 1-km domain has 2149 x 736 grid points. The extent of the domains was also tailored for computational stability.

At present, there are two sets of available land-use data for use in the WRF model: one consists of data produced by the United States Geological Survey (USGS) based on advanced very high-resolution radiation (AVHRR), which contains global imagery from April 1992 to March 1993 and which adopts the USGS's 24 classification categories; the other is the dataset made by the University of Boston based on Moderate-resolution Imaging Spectroradiometer (MODIS) observational data, which

spans from January to December 2001. This latter dataset contains the classifications devised by the International Geosphere Biosphere Program (IGBP), which consists of 20 discrete categories. However, both datasets were generated a long time ago, and since ecosystems and land-use patterns have changed considerably since then, their effectiveness has gradually dwindled over time (after Huoqing Li et. al).

In this research, the Land Use and Soil Categories in the Static Data from MODIS was used. The list of categories is shown in **Table 2** and **Table 3** respectively.

Land Use Category	Land Use Description
1	Evergreen Needleleaf Forest
2	Evergreen Broadleaf Forest
3	Deciduous Needleleaf Forest
4	Deciduous Broadleaf Forest
5	Mixed Forests
6	Closed Shrublands
7	Open Shrublands
8	Woody Savannas
9	Savannas
10	Grasslands
11	Permanent Wetlands
12	Croplands
13	Urban and Built-Up
14	Cropland/Natural Vegetation Mosaic
15	Snow and Ice
16	Barren or Sparsely Vegetated
17	Water
18	Wooded Tundra
19	Mixed Tundra
20	Barren Tundra

Table 2: IGBP-Modified MODIS 20-category Land Use Categorization

Soil Category	Soil Description
1	Sand
2	Loamy Sand
3	Sandy Loam
4	Silt Loam
5	Silt
6	Loam
7	Sandy Clay Loam
8	Silty Clay Loam
9	Clay Loam
10	Sandy Clay
11	Silty Clay
12	Clay
13	Organic Material
14	Water
15	Bedrock
16	Other (land-ice)

Table 3: 16-category Soil Categorization

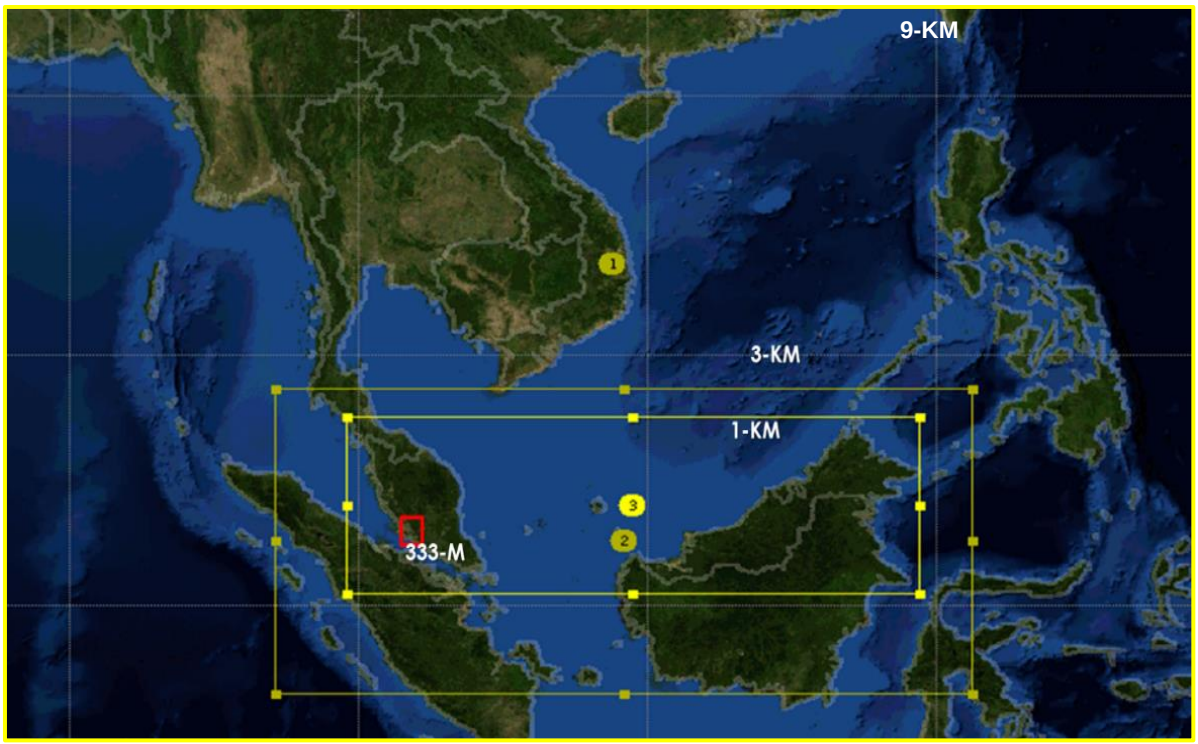

Figure 2: WRF Domain Configuration

3.2 Model Physics

The overall model physics is shown in **Table 4**. If we take a closer look at the model settings, the adaptive time step to ensure the Courant–Friedrichs–Lewy (CFL) condition is complied. The CFL criteria is rather difficult to satisfy for model simulations close to the equator in the tropics. This is due to the horizontally propagating waves and the vertically propagating waves in tropics making numerical stability extremely difficult. Variable time-step is the best option to maintain numerical stability.

Surface layer is a layer most affected by surface in terms of momentum and enthalpy fluxes, and usually the depth of a surface layer is regarded as lower 10% of boundary layer (~10m). The WRF surface physics in this experiment is based on the Monin-Obukhov similarity theory, and the surface fluxes are defined by bulk method. Surface fluxes are proportional to the difference of quantity considered between surface and atmosphere right above, and its exchange coefficient. Because main energy sources and sinks of tropical cyclones are sensible/latent heat fluxes over warm ocean and momentum flux (dissipation) over land, the determination of surface fluxes plays a critical role in predicting accurate hurricane intensity

The Planetary Boundary Layer (PBL) Scheme is used to parameterize sub grid-scale vertical turbulence mixing of momentum, heat, and moisture in the boundary layer. There are two main categories of PBL Schemes, the local and non-local mixing scheme. In the local mixing scheme, vertical mixing is proportional to the local gradient such as the Mellor-Yamada-Janjic (MYJ) scheme and Blackadar Scheme. Whereas the non-local mixing scheme is used when vertical mixing is not only proportional to local gradient but also counter-gradient mixing due to large scale eddy, such as the GFS scheme and Yonsei University (YSU) scheme. We have used and fixed the PBL Scheme to YSU Scheme in all experiments due to the benefits of counter-gradient mixing.

As for the radiative schemes, the Long Wave radiation, the Rapid Radiative Transfer Model (RRTM) was used. RRTM is a rapid radiative transfer model which utilizes the correlated-k approach to calculate fluxes and heating rates efficiently and accurately (Atmospheric & Environmental Research (AER) Radiative Transfer Working Group).

As for the Shortwave (SW) radiation scheme, the Dudhia scheme was used. The Dudhia scheme technically performs better during cloudless conditions (Zempila et. al). These parameterization settings have been kept without change for all simulations.

When grid resolution of a numerical model is too coarse to resolve individual convection, there is need to parameterize the impact of convection to grid scale. Convection does stabilize the atmospheric column by vertical transportation of heat, moisture, and momentum. There are two main categories in convective parameterization scheme. One is an adjustment scheme and the other is a mass flux scheme.

The 9-km Domain 1 was fixed using the Betts – Miller – Janjic (BMJ) and the 3-km Domain 2 in the WRF model experiment were simulated using a combination of cumulus parameterization schemes based on the, Grell – Devenyi (GD), Simplified Arakawa – Shubert (SAS), Kain – Fritsch new ETA (KF-eta) and Tiedtke Scheme to evaluate the sensitivity of precipitation forecasts. The combinations of the selected schemes are indicated in **Table 5**.

Table 4: WRF Model Configuration

Physical processes	Domain 1 (9 km)	Domain 2 (3km)	Domain 3 (1 km)	Remarks
Dimensions	368 X 368 (with 51 vertical levels)	886 X 442 (with 51 vertical levels)	2149 X736 (with 51 vertical levels)	Arakawa-C Grid Non-hydrostatic WRF v4.2 model Mercator projection Hourly forecast for a forecast range of 60 hours
Time interval (Δt)	36 - 108 sec (Adaptive Time step)	12 -36 sec (Adaptive Time step)	4 - 12 sec (Adaptive Time step)	
Cumulus Parameterization	BMJ	• Betts – Miller – Janjic (BMJ)Grell – Freitas (GF) • Simplified Arakawa – Shubert (SAS) • Kain – Fritsch new ETA (KF-ETA) • Grell-Devenyi Ensemble Scheme (GD)	None	
Microphysics	WSM 6	WSM 6	WSM 6	
PBL	YSU scheme	YSU scheme	YSU scheme	
Radiation	RRTM / Dudhia scheme	RRTM / Dudhia scheme	RRTM / Dudhia scheme	
Land Use	MODIS 5 minute	MODIS 2 Minute	MODIS 30 Sec	
Surface-Physics	5-layer Thermal Diffusion Scheme	5-layer Thermal Diffusion Scheme	5-layer Thermal Diffusion Scheme	
Initial and Boundary data	GFS / UM	WRF 9 km	WRF 3 km	

Table 5: The various cumulus parameterization schemes used for different domains in each simulation.

Domain / Experiment	1 (9 km)	2 (3 km)
A	NC	NC
B	BMJ	BMJ
C	BMJ	NEW TIEDTKE
D	BMJ	NC
E	BMJ	KF – ETA
F	BMJ	GD
G	BMJ	GF
H	BMJ	SAS

Notes:

- No Cumulus Scheme (NC)
- Betts – Miller – Janjic (BMJ)
- Grell – Freitas (GF)
- Simplified Arakawa – Shubert (SAS)
- Kain – Fritsch new ETA (KF-ETA)
- Grell-Devenyi Ensemble Scheme (GD)

KF - ETA is a mass-flux scheme used for moisture updraft and downdraft. This scheme incorporates a trigger function to initiate convection, thus compensating for circulation, and closure assumption (Kain and Fritsch 1993; Kain 2004).

BMJ is a convective adjustment scheme. This scheme was developed to adjust atmospheric instabilities based on a reference climatological profile. It triggers deep convection when sufficient moisture is available (Betts and Miller 1986; Janjić 1994).

GF (GF; Grell and Freitas 2014) is an ensemble scheme, in which multiple cumulus schemes and variants are run within boxes to obtain an ensemble-mean realization. The ensemble members use different parameters for updraft/downdrafts entrainment/detrainment. It is an updated Grell–Dévényi scheme (Grell and Dévényi 2002), such that the scale awareness is improved by introducing the method of Arakawa et al. (2011). This relaxes the assumptions of traditional parameterizations in which convection is contained within individual model grid columns when the fractional area covered by convection clouds is small (Raju Attada et. al).

Grell and Devenyi (2002) introduced an ensemble cumulus scheme in which effectively multiple cumulus schemes and variants are run within each grid box and then the results are averaged to give the feedback to the model. In principle, the averaging can be weighted to optimize the scheme, but the default is an equal weight. The schemes are all mass-flux type schemes, but with differing updraft and downdraft entrainment and detrainment parameters, and precipitation efficiencies. These differences in static control are combined with differences in dynamic control, which is the method of determining cloud mass flux. The dynamic control closures are based on convective available potential energy (CAPE or cloud work function), low-level vertical velocity, or moisture convergence. Those based on CAPE either balance the rate of change of CAPE or relax the CAPE to a climatological value or remove the CAPE in a convective time scale. The moisture convergence closure balances the cloud rainfall to the integrated vertical advection of moisture. Another control is the trigger, where the maximum cap strength that permits convection can be varied. These controls typically provide ensembles of 144 members.

The Simplified Arakawa Shubert (SAS) a mass flux schemes. This group of schemes is based on simplified Arakawa-Schubert scheme (SAS) (Grell, 1993) which considers only one type of cloud instead of an ensemble. They all use the quasi-equilibrium closure. They vary by how they handle convective downdrafts, shallow convection, momentum transport (all three not included in the original AS and last two not in SAS), entrainment/detrainment and scale-aware aspects. In the SAS scheme, a parcel lifted from the updraft-originating level must reach its level of free convection (LFC) within a critical depth for convection to occur. In the original scheme, the critical depth is determined in proportion to the large-scale vertical velocity at the cloud base to produce more convection in large-scale convergent regions (Han and Pan 2011)

The Tiedtke scheme is a mass-flux scheme, and it parameterizes deep, shallow and midlevel convection. It represents the cloud ensemble by a bulk cloud model, and considers entrainment and detrainment and downdrafts. It uses a CAPE closure to determine the strength of the deep and midlevel convection, and surface evaporation for shallow convection. In the version implemented in WRF (Zhang and Wang, 2011), turbulent entrainment and detrainment are added and turbulent entrainment for shallow convection is increased to promote boundary layer cloud formation. Another

modification is to change how detrained cloud at the top is treated: in the original scheme, it evaporates immediately; and in the current scheme, it is added to the grid scale. To limit the deep convection in drier regions, a minimum relative humidity of 80% is imposed for the mean RH between cloud base and top.

The New Tiedtke Scheme is an updated version of the Tiedtke scheme, and it is closer to the one used in the recent ECMWF IFS (Zhang and Wang, 2017). The updates include trigger functions for deep and shallow convection, closures for deep and shallow convection, convective adjustment time scale, entrainment and detrainment rates for all types of convection, conversion from cloud water/ice to rain/snow and options for momentum transport.

Both the Tiedtke Schemes are based on a entraining and detraining plume model which considers three different types of convective parameterizations. The cloud base and cloud tops are determined by use of parcel method. This scheme is highly simplified microphysical parameterizations for both organized and turbulent entrainment and detrainment considerations.

While convective parameterization scheme is parameterizing sub grid/unresolvable moist processes, microphysics scheme predicts the behavior of hydrometeor species explicitly. Hence, microphysics schemes are called explicit moisture scheme, grid scale precipitation scheme or large-scale precipitation scheme. There are bulk microphysics schemes (which are widely used in NWP models) and bin microphysics schemes.

We have considered the WSM6 scheme in this research. WSM6 is a six-class scheme which extends the WSM5 scheme to include graupel and its associated processes. Some of the graupel-related terms follow Lin et al. (1983), but its ice-phase behavior is much different due to the changes of Hong et al. (2004). A new method is introduced for representing mixed-phase particle fall speeds for the snow and graupel particles by assigning a single fallspeed to both that is weighted by the mixing ratios and applying that fallspeed to both sedimentation and accretion processes (Dudhia et al., 2008). The behavior of the WSM3, WSM5, and WSM6 schemes differ little for coarser mesoscale grids, but they work differently on cloud-resolving grids. Of the three WSM

schemes, the WSM6 scheme is the most suitable for cloud-resolving grids, considering the efficiency and theoretical backgrounds (Hong and Lim, 2006). All of the WSM schemes compute effective radii for ice, snow and cloud water to interact with RRTMG radiation.

3.3 Initial and Boundary Conditions

To generate both initial and boundary conditions, GFS forecasts are used, with a horizontal resolution of 0.25 X 0.25-degree latitude/longitude) and a 6-hour time interval between two consecutive forecast outputs. Specifically, to initialize a WRF simulation at 00 or 12Z, GFS forecasts initialized 12 hours earlier have been used. Consequently, the first guess is generated from a GFS 12-hour forecast and subsequent 6-hour forecasts are used to provide boundary conditions for the coarsest domain. For simulations in nested domains, both initial and boundary conditions are supplied from their parent domain's run. All 9 km, 3 km and 1 km simulations are initialized at the same time as the coarsest domain run.

4.0 Selected Rainfall Episodes

During the early boreal winter (northeast) monsoon (November–December), cold air frequently bursts out from intense Siberian highs toward the Chinese coast in response to the development and movement of a 500-hPa trough. The resultant strong low-level northwesterlies turn into northeasterlies across the South China Sea as ‘‘cold surges.’’ On interacting with the near-equatorial trough, mesoscale convective systems form north of the trough, normally giving rise to heavy downpours and severe flooding, mainly along the coastal stretch in the east coast states of Peninsular Malaysia (Ooi See Hai, 2017 et. al).

Heavy rainfall associated with three surges during the 2008/2009 Northeast monsoon were selected for the case study. These cases were simulated using WRF with varying Cumulus Parameterization Schemes as explained in Section 3.0. The retrospective cases were selected to gauge the current model performance on the event in the past and the sensitivity associated with parameterization schemes.

The events considered took place on the **29 November – 1 December 2008 (Case 1)**, **5 – 7 December 2008 (Case 2)** and **24 – 26 December 2008 (Case 3)**. These events were characterized by cold air burst from Siberia (cold surge) bringing a lot of rainfall to northeast coast states of Kelantan and Terengganu. These heavy rainfall episodes lasted mainly for about three to four days.

4.1 Observed vs Satellite Rainfall

The rainfall pattern in Case 1 is shown in **Figure 3A** and **3B. Figure 3A** shows the 24-hour accumulated rainfall from the 29 November 2008 to 1 December 2008. The peak rainfall primarily was over the inland of Kelantan and was captured by the meteorological stations and also the Satellite data from Tropical Rainfall Measuring Mission Satellite (TRMM). On the 29 November the Klang Valley region also received quite a lot of rainfall. The heavy rainfall continued to the 30 November and 1 December however the rainfall on the 30 November and 1 December was more towards the coastal regions. Over Sabah and Sarawak, the Satellite data could not pick up the peak rainfall clearly compared to the Station data, however the peak mainly was over Kuching as depicted in **Figure 3B**. There are disparities based on the TRMM and the station observed rainfall but the signals are in consensus and both these data tend to complement each other. We have used both these data sets to analyze the rainfall pattern during the heavy rainfall episode.

In Case 2 as shown in **Figure 4A** and **4B,** The rainfall peak on the 5 and 6 December is concentrated mainly on the Northeast coast of Peninsula Malaysia and centered inland areas and encompassing both Kelantan and Terengganu. On the 7 December the rainfall was more towards Kuantan and Southern Terengganu. As for Sabah and Sarawak, if take a look at the Station data , the rainfall peak on the 5 December is more in Brunei and central Sarawak on the 6 December. The satellite rainfall does not show much rainfall except for the 5 December over Brunei.

Case 3 rainfall distribution over the heavy rainfall period is shown in **Figure 5A** and **5B**. The heavy rainfall on the 24 December was over the Northeast and Northwestern Peninsula Malaysia with the Northwestern part receiving more rainfall. However, on the 25 and 26 December the northeast coast began receiving more rainfall. Over

Sabah and Sarawak, the heavy rainfall was focused more over western Sarawak from the 24 – 26 December.

The rainfall pattern in all three cases is consensus with the northeast monsoon dynamics and the rainfall characteristics are primarily driven by the monsoon trough and the cold surges. The synoptics and dynamics will be explained in the next section. Moisture convergence due to the cold surges and broad easterlies had brought heavy rainfall to the northeast coast on the 28 November, 5 December and 24 December 2008. How far the convergence progressed in land depended on the easterlies pushing in the moisture. The heavy rainfall episodes in all the cases lasted approximately three to four days with the peak occurring within three days. The peak 24 – hour accumulated rainfall was around 60 – 200 mm in these cases.

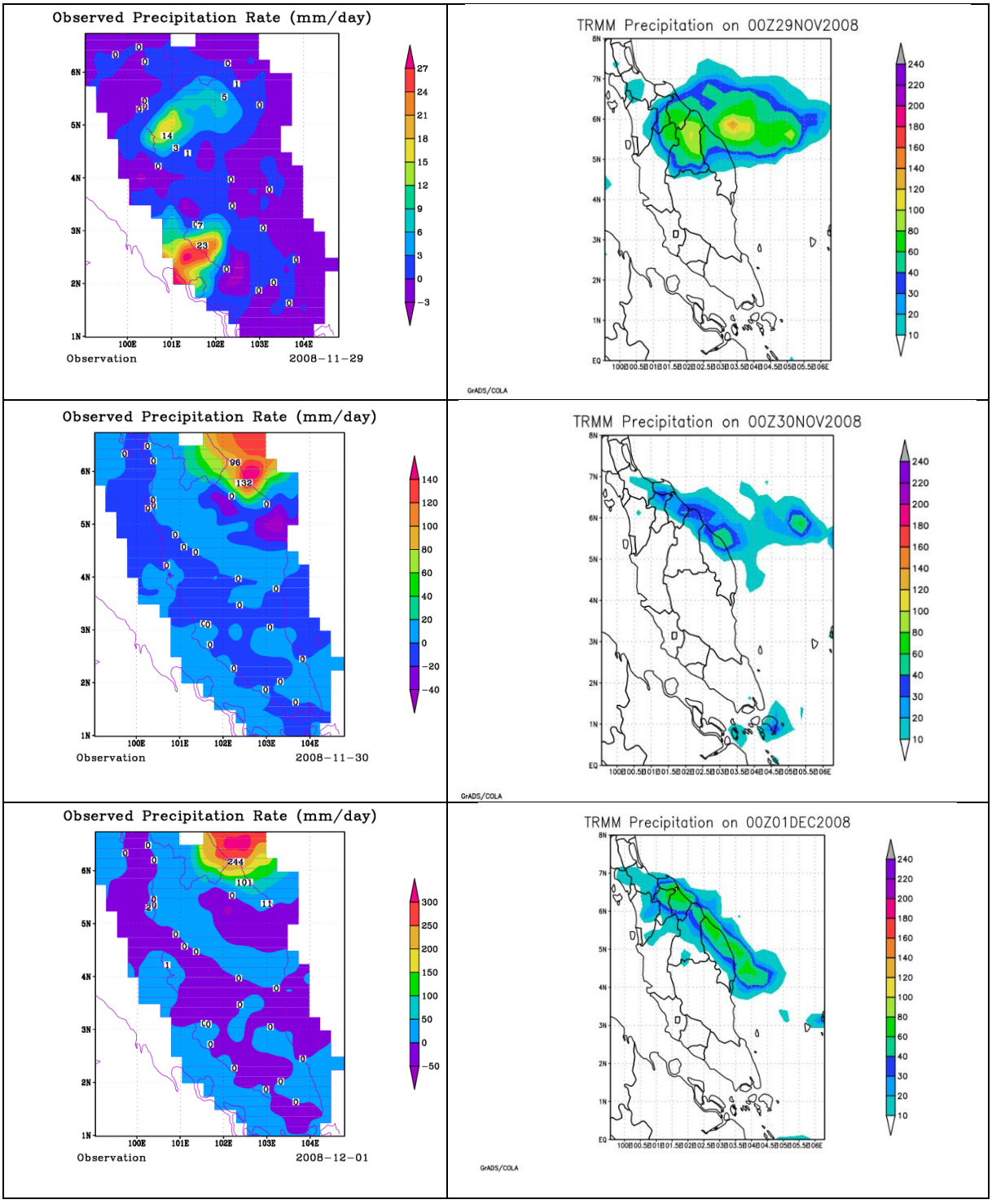

FIGURE 3A: Meteorological Station and TRMM Satellite Precipitation rate (mm/day) over Peninsular Malaysia from 29 November 2008 - 1 December 2008 (Case 1).

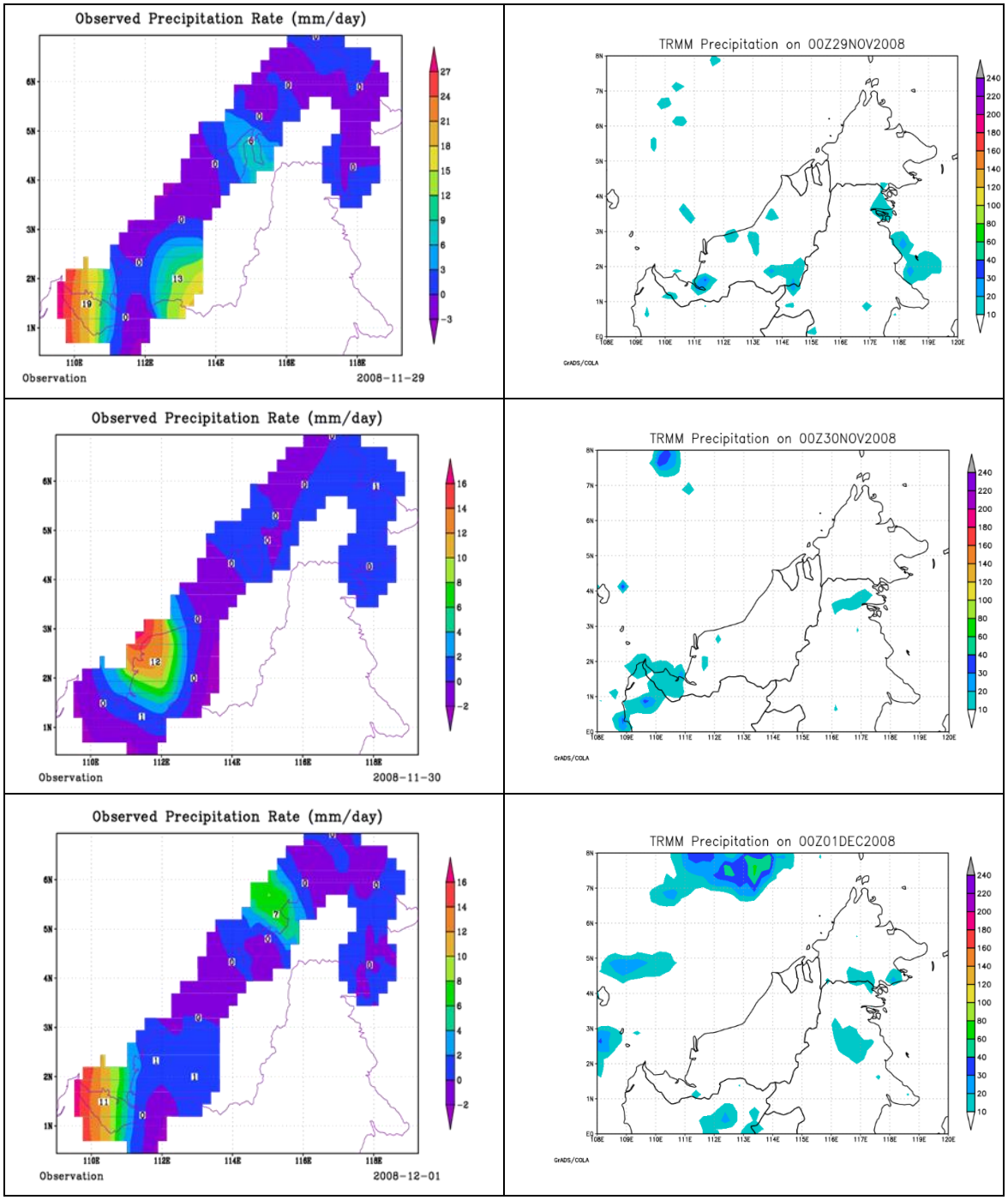

FIGURE 3B: Meteorological Stations and TRMM Satellite Precipitation rate (mm/day) over Sabah and Sarawak from 29 November 2008 - 1 December 2008 (Case 1).

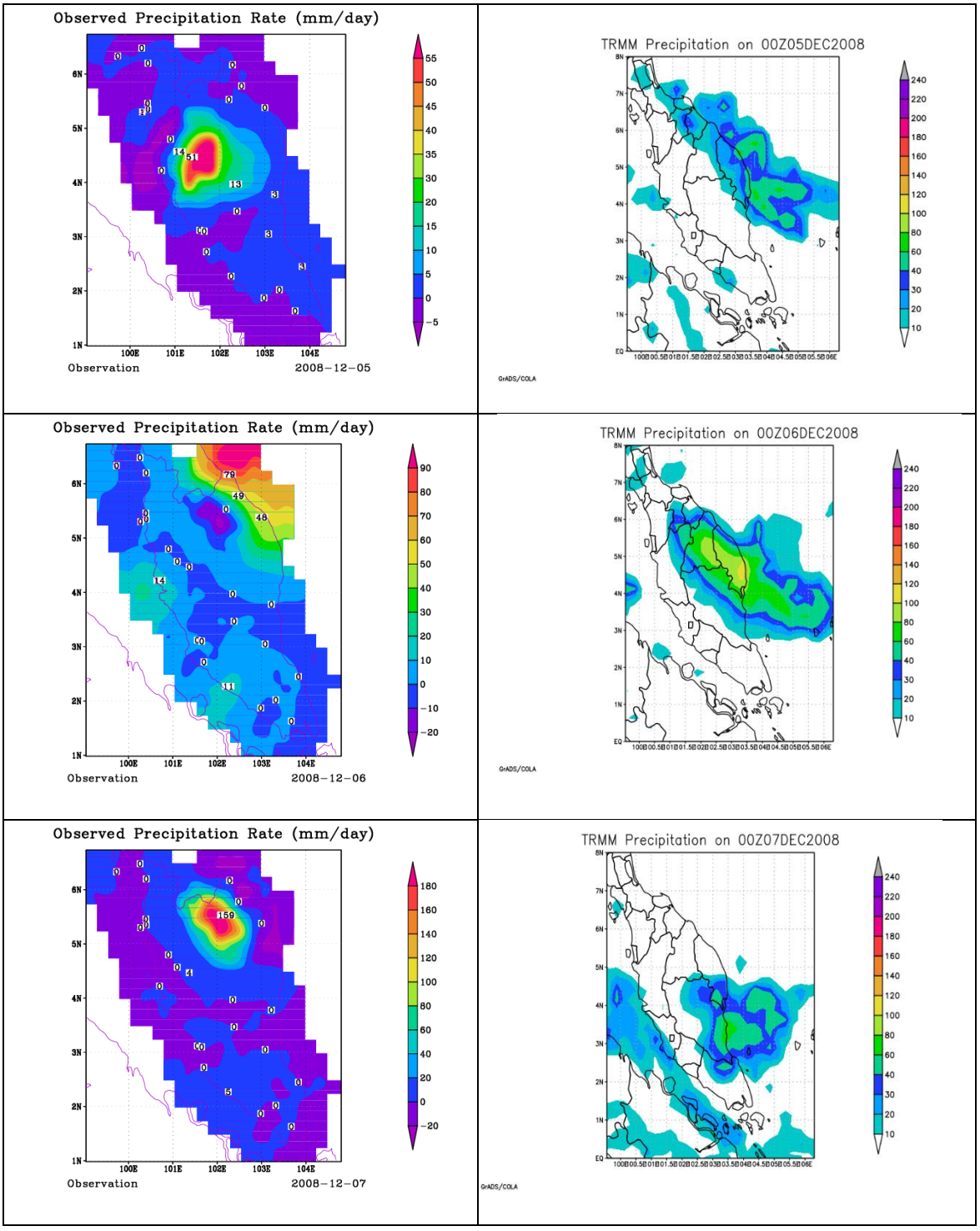

FIGURE 4A: Meteorological Station and TRMM Satellite Precipitation rate (mm/day) over Peninsular Malaysia from 5 - 7 December 2008 (Case 2).

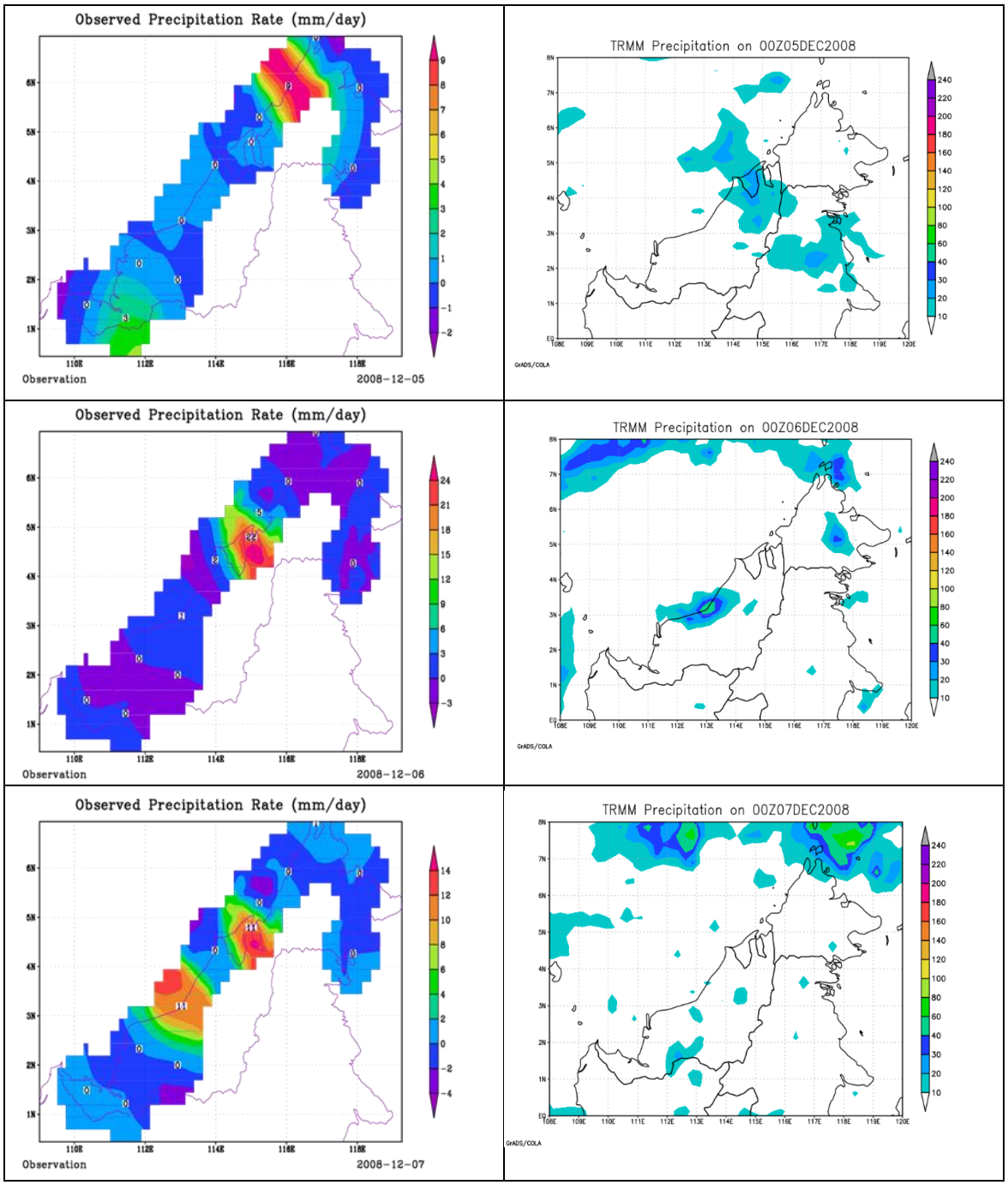

FIGURE 4B: Meteorological Stations and TRMM Satellite Precipitation rate (mm/day) over Sabah and Sarawak from 5 - 7 December 2008 (Case 2).

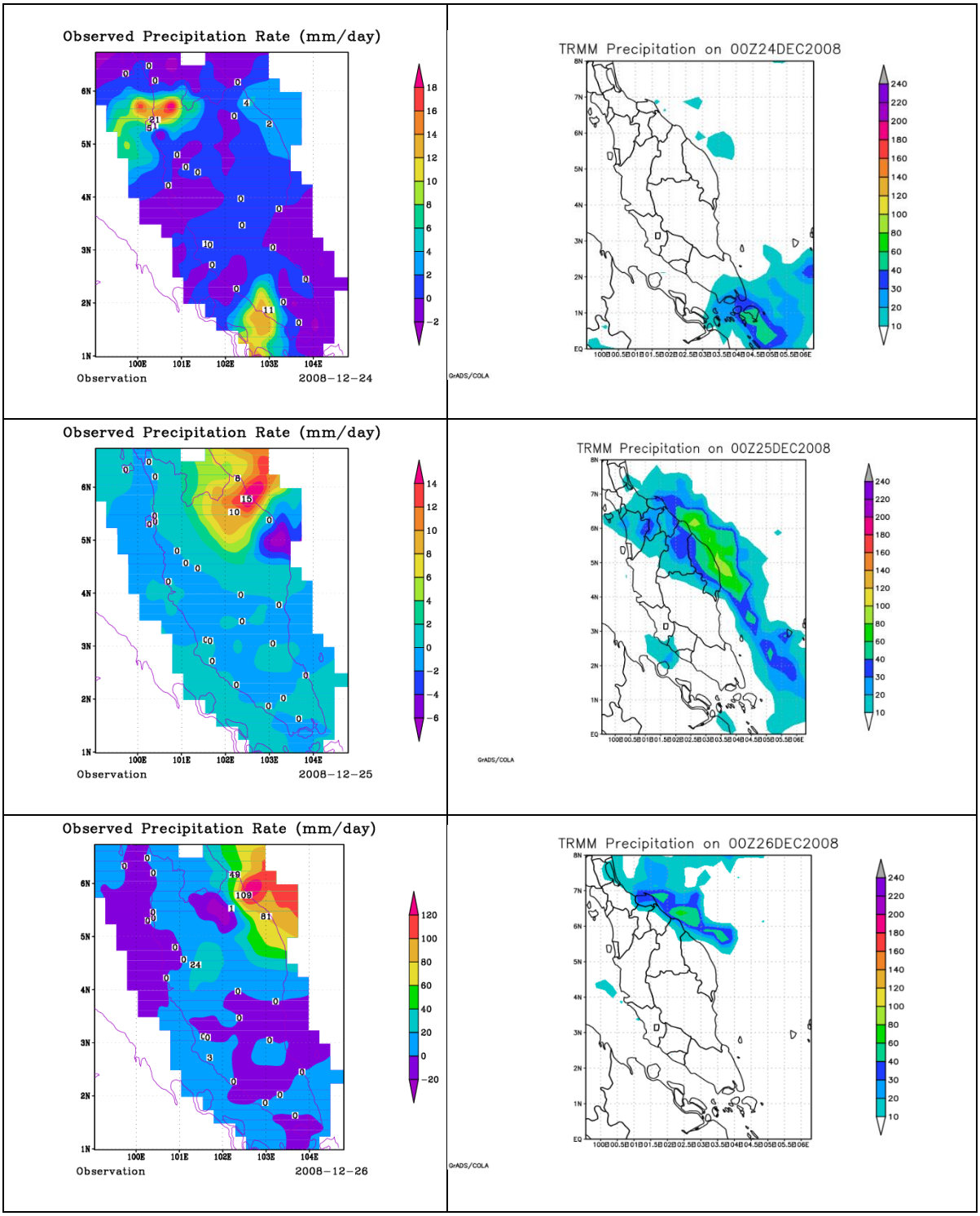

FIGURE 5A: Meteorological Station and TRMM Satellite Precipitation rate (mm/day) over Peninsular Malaysia from 24 - 26 December 2008 (Case 3).

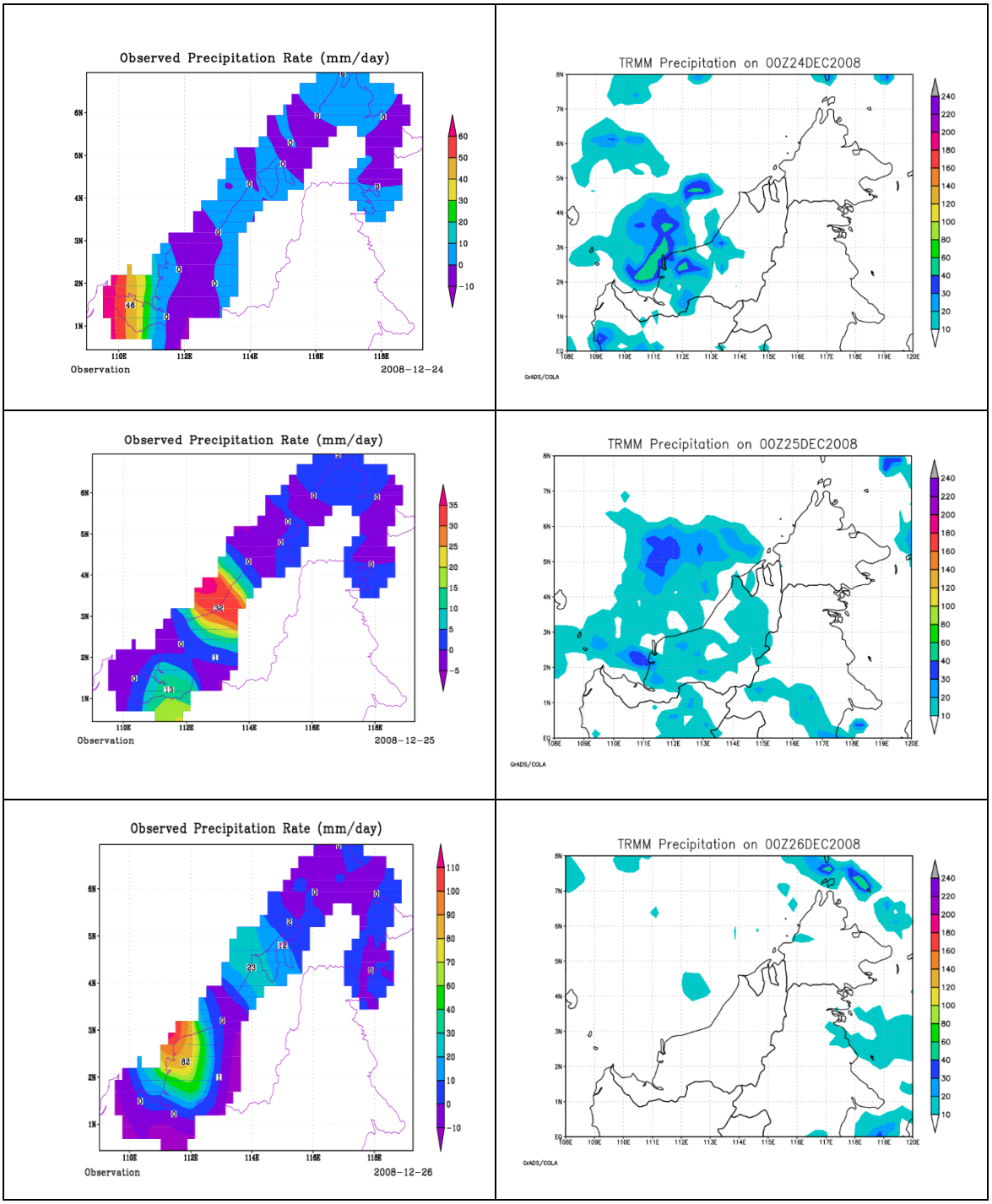

FIGURE 5B: Meteorological Stations and TRMM Satellite Precipitation rate (mm/day) over Sabah and Sarawak from 24 - 26 December 2008 (Case 3).

4.2 Major Synoptic Features

The general monsoon circulation is represented in **Figures 6A** and **6B.** If we take a closer look at the general circulation pattern, all the three cases we in line with the climatology making these events predictable however the lead time and the intensity of the forecast rainfall defers and is sensitive to the model physics.

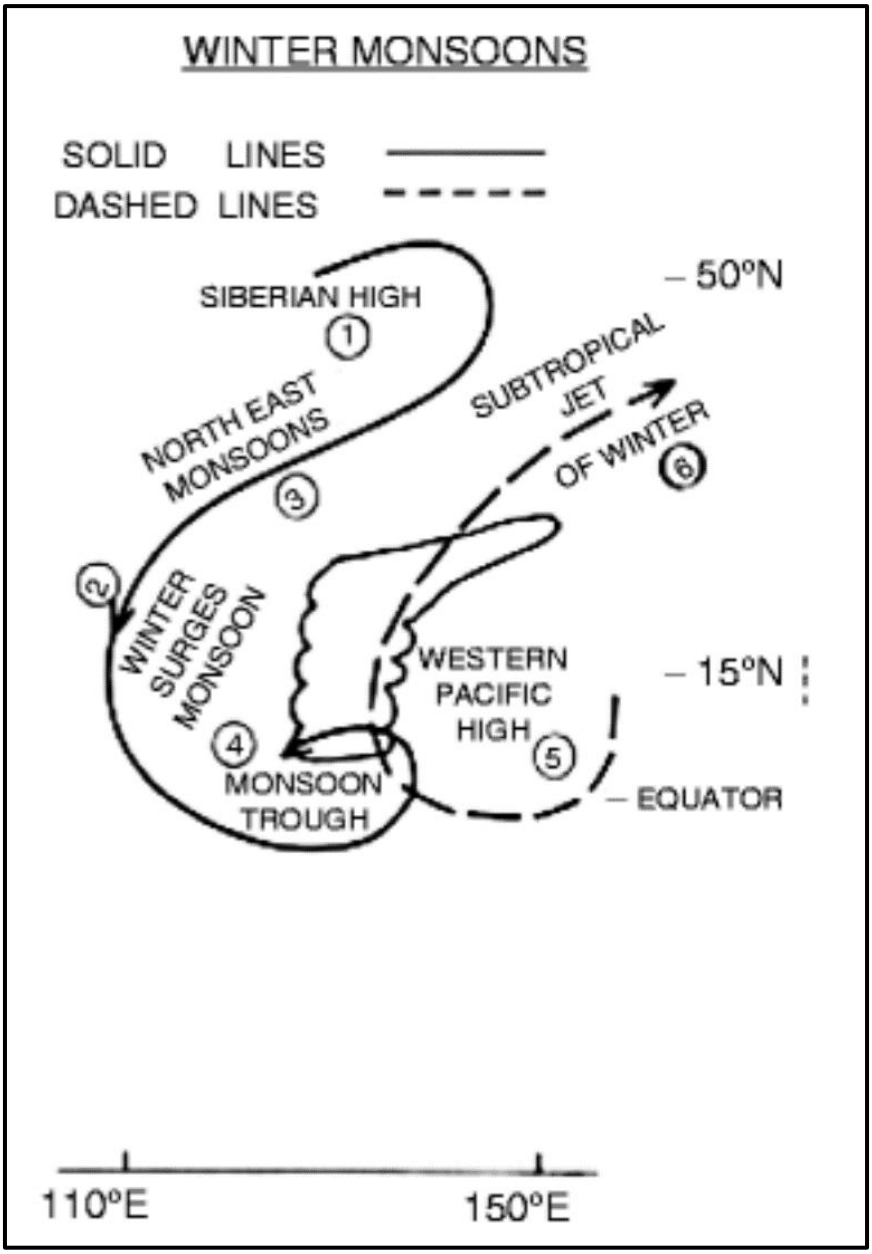

FIGURE 6A: Northeast Monsoon Conceptual Diagram. Solid Lines indicates surface processes and dashed line indicates upper air processes.

In **Figure 6A,** the Siberian high-pressure system also known as the Siberian high is. climatologically located near 50 ° N and 125 ° E. This is a region of significant heat sink in the troposphere of the northern hemisphere during winter. The Northeast monsoon is characterized by the northeasterly lower tropospheric flow. Wind surges carried by the northwesterly monsoonal flow seen along the western shores of the South China Sea. The winds in these surges can be as strong as 15 m/s, and are normally associated with cyclonic disturbances in the central part of the South China Sea.

The Monsoon trough, located north of the equator in December and south of the equator in the months of January and February. The Monsoon trough is the locale of the heavy rains of the Winter Monsoon over Southern Peninsular Malaysia and Borneo. The West Pacific high is a counterpart to the Tibetan high. It resides over the region of heavy monsoon rains and is strongest near the 200 mb level. The subtropical jet stream of winter (STJW). This is one of the strongest wind systems of the troposphere. It is located near the northern flanks of the West Pacific high, south of Japan.

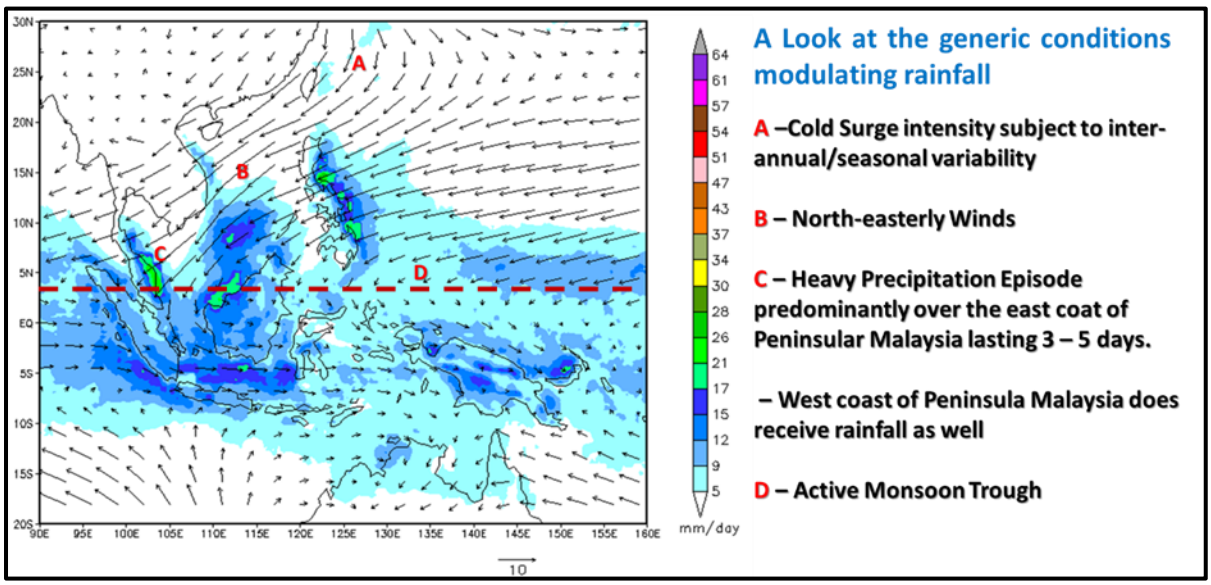

FIGURE 6B: Major features of the Northeast Monsoon over the Malaysian region. Image cutesy of Yip et. al.

With reference to **Figure 6B**, the position of the monsoon trough in November is slightly to the north of Peninsula Malaysia as compared to December. This trough is

active during this period and coupled with cold surges, produces heavy precipitation episodes lasting 3 to 5 days as seen in the three selected case studies.

Figure 7 shows the meridional pressure gradient between Wuhan - Hong Kong, Hong Kong – Kota Bahru and Wuhan – Kota Bahru for all 3 cases. The pressure build-up and the presence of broad easterlies played an important role in modulating rainfall in all three cases. In all three cases there is a significant meridional pressure difference indicating the strong meridional cold surge. The cold surge coupled with the air-sea interaction over the South China Sea, feeds moisture to the northeast coast creating heavy rainfall episodes during the cases. In Case 1 , the pressure difference peaked on the 27– 28 November, thus the cold air burst from Siberia began during this period reaching Kota Bahru by the 28 November.

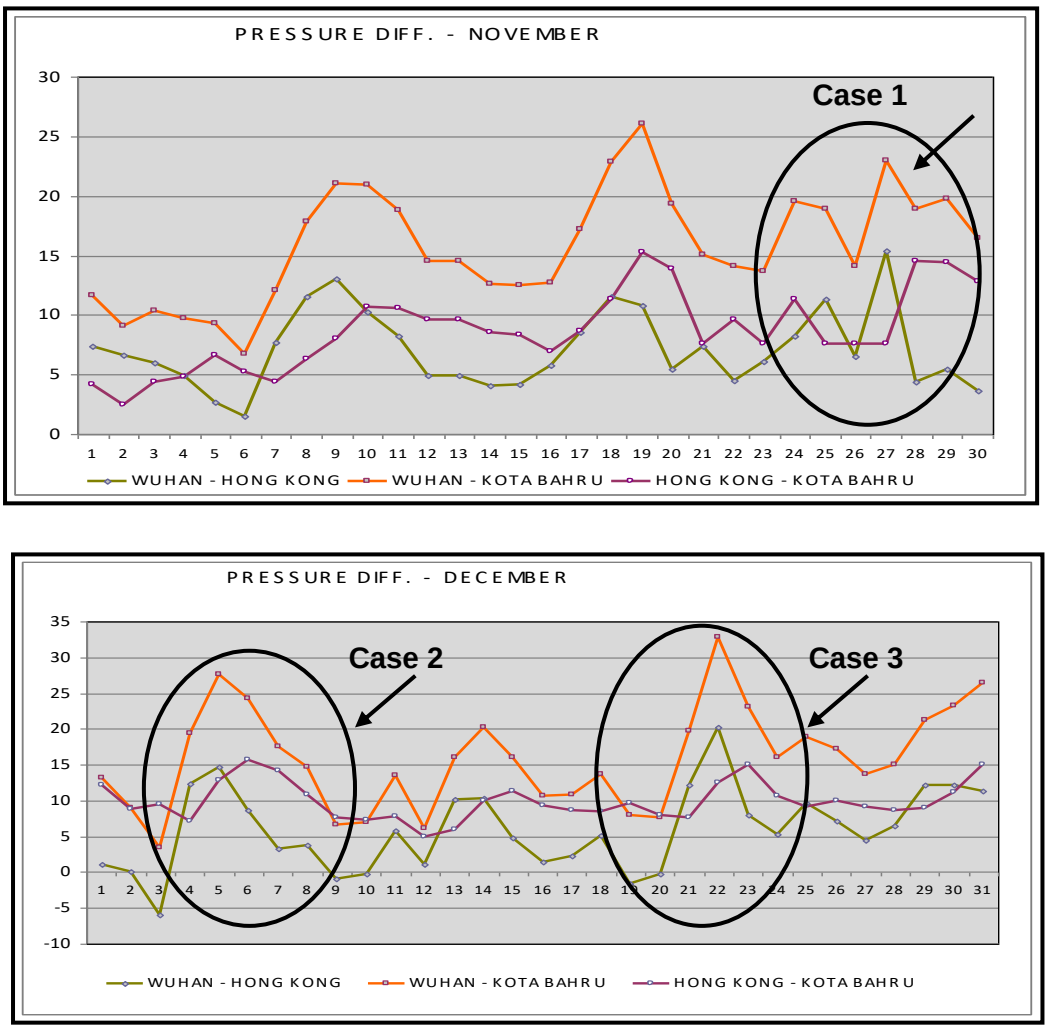

FIGURE 7: MSLP Difference between Wuhan – Hong Kong, Wuhan – Kota Bharu and Hong Kong – Kota Bahru for November and December 2008. The location of Hong Kong, Wuhan and Kota Bharu is shown in

In Case 2, the peak build up was on the 5 December , creating the cold air burst and for Case 3 , the peak pressure gradient was on the 23 December. These were consistent with the Cold Surge occurrence.

We have also plotted the Meridional Surge Index (MSI) and the Easterly Surge Index (ESI) (Fakaruddin et. al) to further explain the conditions which brought about the heavy rainfall episode in **Figure 8A** and **8B**. From **Figure 8A**, A Cold Surge episode is said to begin when the index is less than -8 m/s for 3 consecutive days and ends when the index goes above -8 m/s for at least 3 consecutive days. (An average of 925-hPa meridional wind of 110-117.5°E along 15°N). An easterly surge episode is said to begin when the index is less than -8 m/s for 3 consecutive days and ends when the index goes above -8 m/s for at least 3 consecutive days. (An average of 925-hPa zonal wind of 7.5-15°N along 120°E). While for Mixed Surge it occurs for 2 consecutive days.

A further look at the MSI and the ESI, MSI was intense for Case 1 and Case 2 compared to Case 3. ESI was prevalent in Case 3. In Case 1 the meridional surge was most prevalent. In case 3 the easterly surge was more prevalent. In Case 2 there was a combination of both the meridional and easterly surge.

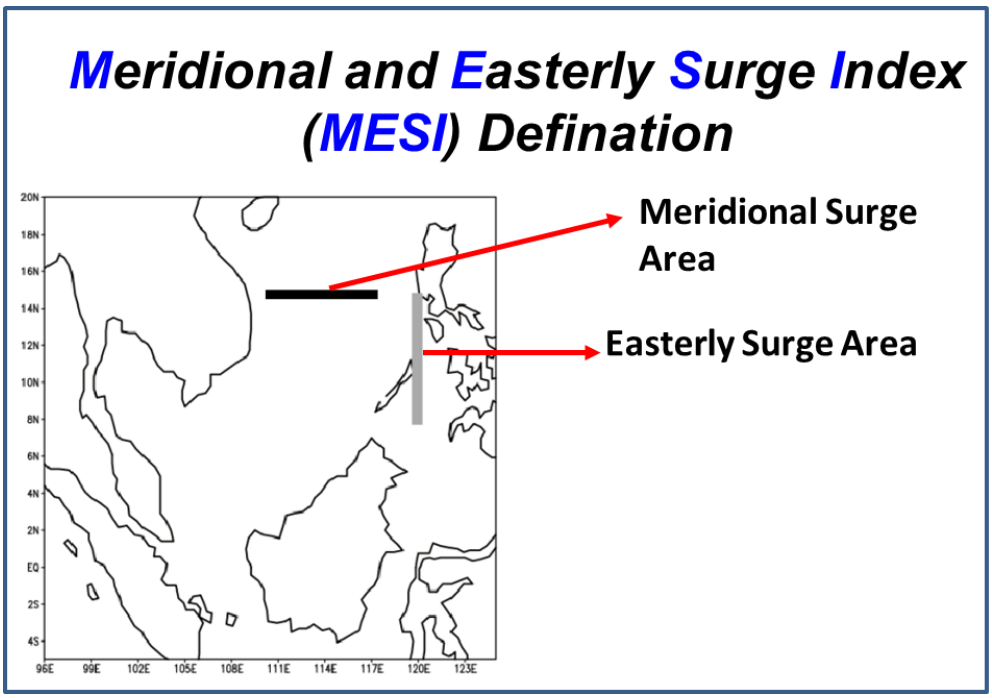

FIGURE 8A: Definition of Meridional and Easterly Surge. Image courtesy of Fakaruddin et. al.

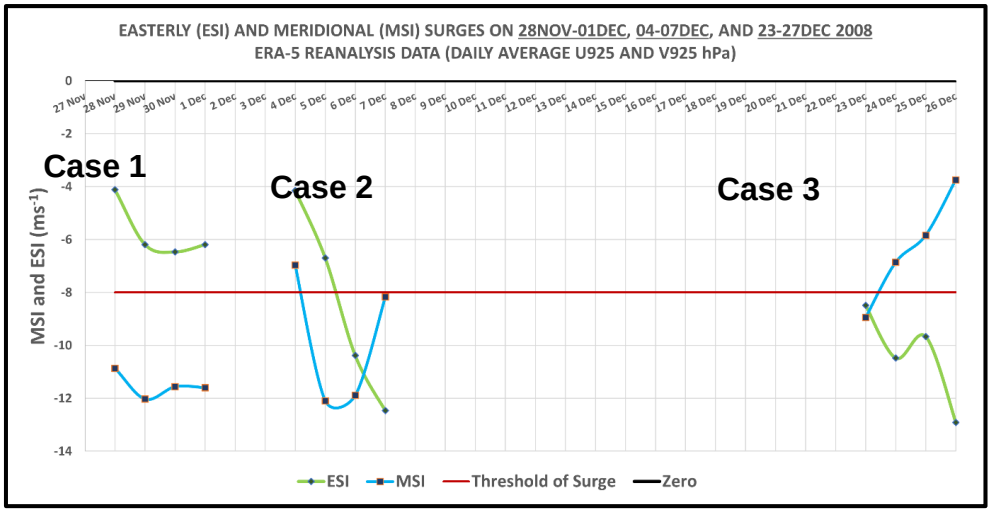

FIGURE 8B: Meridional and Easterly Surge Index during the selected cases. Image courtesy of Diong et. al

Figures 9A, **B** and **C** indicate the synoptic conditions during the three events respectively. We will use the Gradient wind idea by Carl Gustaf Rossby et. al (1939) to further illustrate the retrogression of the Rossby waves at 500 hPa. Case 1 is depicted in **Figure 9A**. On the 28 November the 500 hPa Geopotential height (GPT) trough/ridge system began to move eastwards, and, on the 29 November, the surface winds began enhancing and the strong Northeasterly wind convergence begam to occur. On the 1st of December the isopleths of GPT began to flatten and the northeasterly winds began slowing down. The rainfall associated with the strong north easterly winds are shown as well.

Case 2 is shown in **Figure 9B**. The pressure builds up in Case 2 was rather high with the 500 hPa GPT tightening and progressing eastwards causing very strong broad easterly winds, hence modulating the easterly surge. The position of the GPT isopleths also indicated the strong north easterlies converging on Kota Bahru as indicated by the TRMM satellite imageries. This case had both the meridional and the easterly surges spawning from the strong pressure buildup over Siberia. On the 7th of December the 500 hPa GPT begins to flatten out showing the end of the surge episode.

A look at Case 3 as depicted in **Figure 9C,** the movement of the 500 hPa trough further east indicates the presence of easterly surge coupled with broad easterlies. The

isopleths of GPT tightened on the 25 December, causing strong easterly winds converging over Kota Bahru creating heavy rainfall.

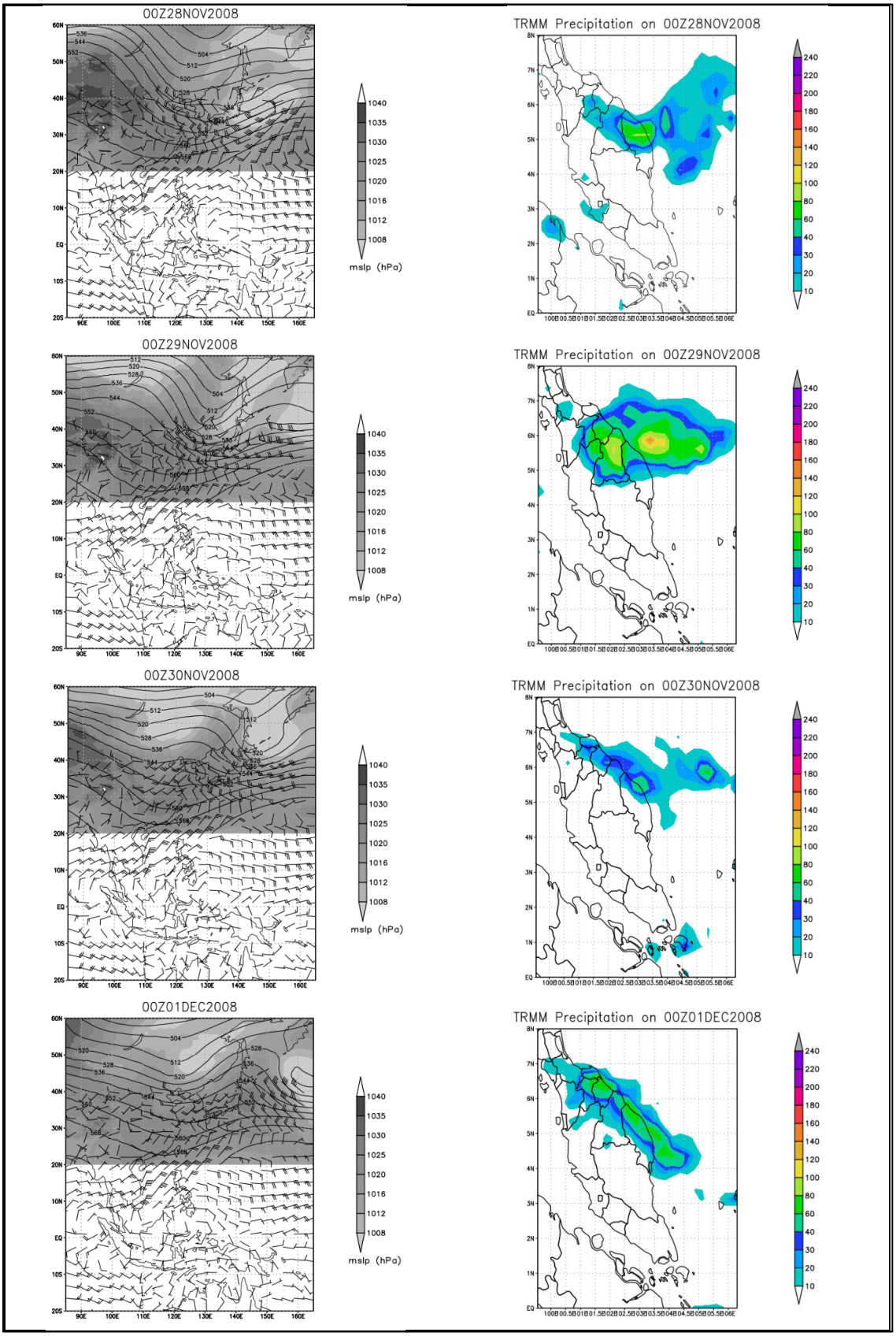

FIGURE 9A: Synoptic Situation and TRMM Satellite Imageries for Case 1

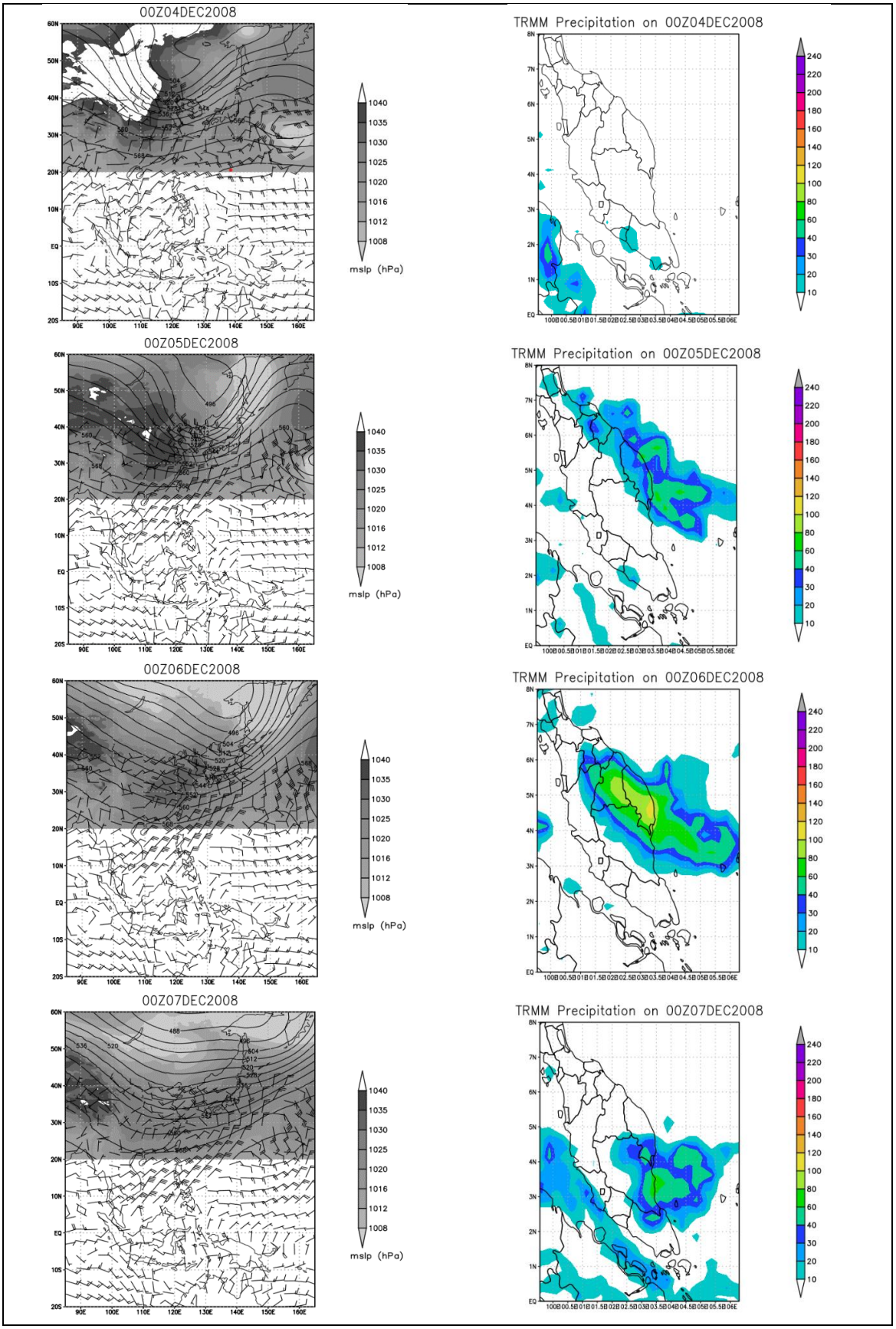

FIGURE 9B: Synoptic Situation and TRMM Satellite Imageries for Case 2

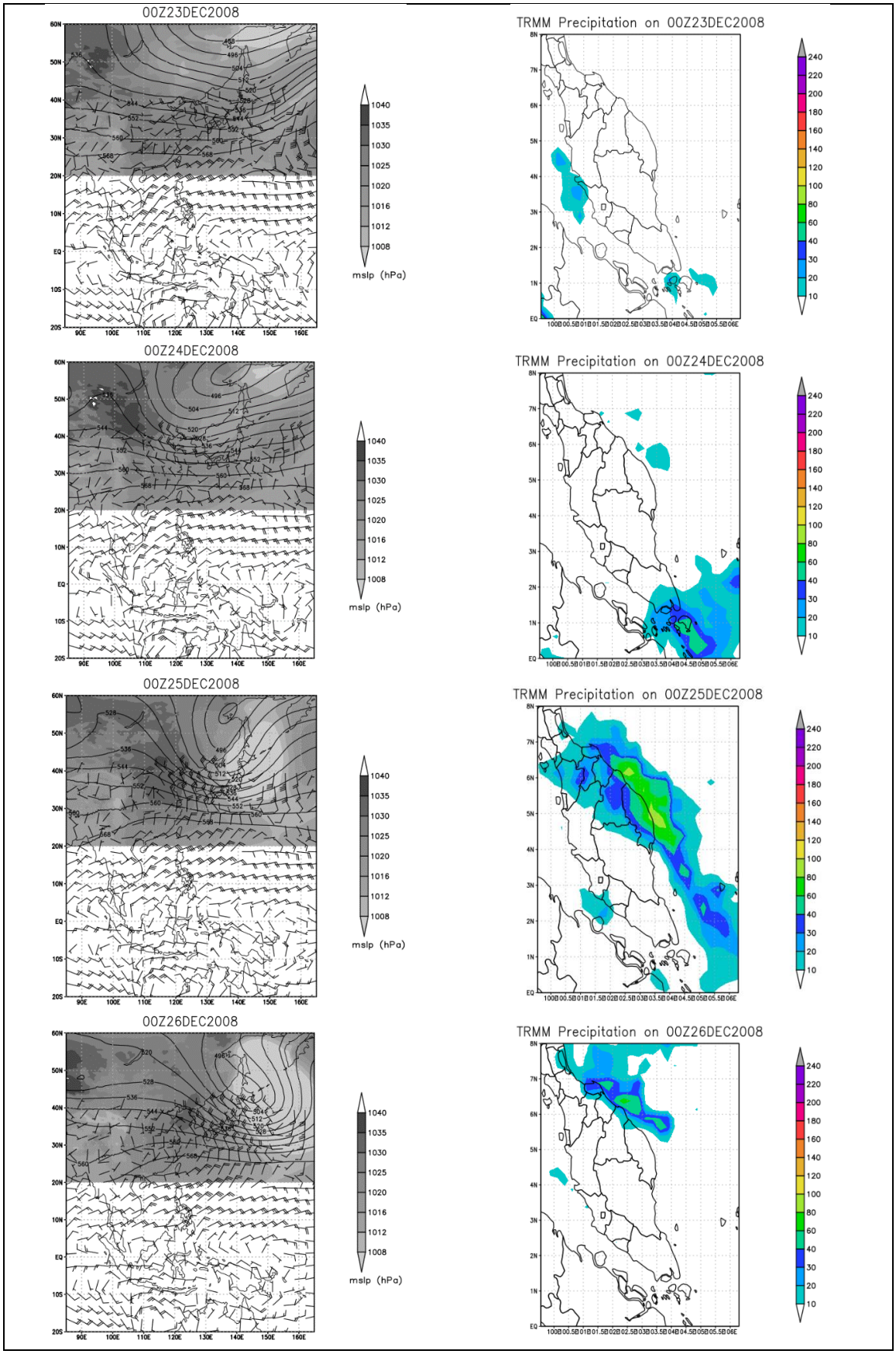

FIGURE 9C: Synoptic Situation and TRMM Satellite Imageries for Case 3

5.0 Results and Discussion

The verification for the 24-hour accumulated rainfall for the experiments on **Table 5** was performed and the results are shown in **Figures 10A**, **10B** and **10C**. BMJ was fixed for the outer 9-km Domain and the simulation results for the 3-km domain was verified based on the meteorological station data.

Figure 10A indicates that all combinations did not perform well for L, M, H and S rainfall thresholds on the 29 November. However, Experiment C yielded a high skill score for T threshold which is rainfall exceeding 100 mm/day. Whereas on the 30 November and 1 December, all combinations performed rather well for M, H and S thresholds. All simulations still did not perform for the L threshold. Experiment C and E performed better for the M, S and T threshold.

We noticed that the BMJ-Tiedtke combination performed well for all thresholds except the low rainfall threshold. BMJ suites well for the coarser outer domain of 9-km whereas the Tiedtke scheme does well for the inner 3-km domain. The combination of the WSM 6 and the BMJ-Tiedtke Scheme had performed well with ETS scores above 0.2.

The beginning of the heavy rainfall period on the 29 November was not captured by all model except for the experiment C which performed well for the higher T threshold. As the days progressed, the other simulations did pick up the signals and did perform reasonably well, however Experiment C stood out compared to the rest of the simulations.

In Case 2 (refer **Figure 10B**), the initial phase was not well captured by all simulations except for Experiment C and H. However, on the 6 December all simulations performed well for the higher rainfall thresholds. On the 7 December, Experiment performed well for M, H and S threshold.

In Case 3, **Figure 10C** indicates that all the simulations performed well for the H, S and T thresholds. However, the lower threshold was not represented well by any of the model simulations. Experiment C and H were the only simulations to perform well on the 26 December towards the tail end of the heavy rainfall episode for threshold H.

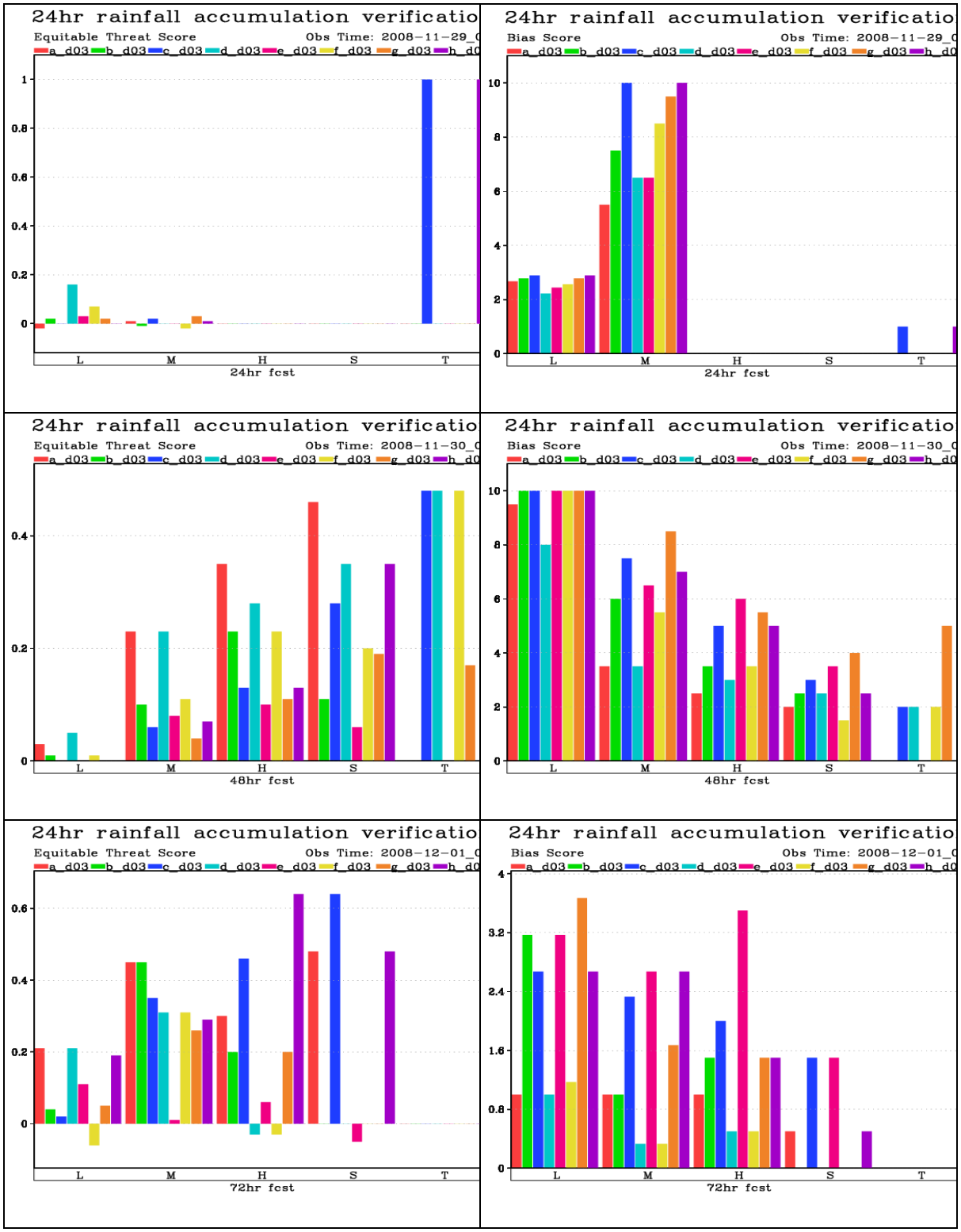

FIGURE 10A: ETS and Bias Scores for Case 1 over Peninsular Malaysia

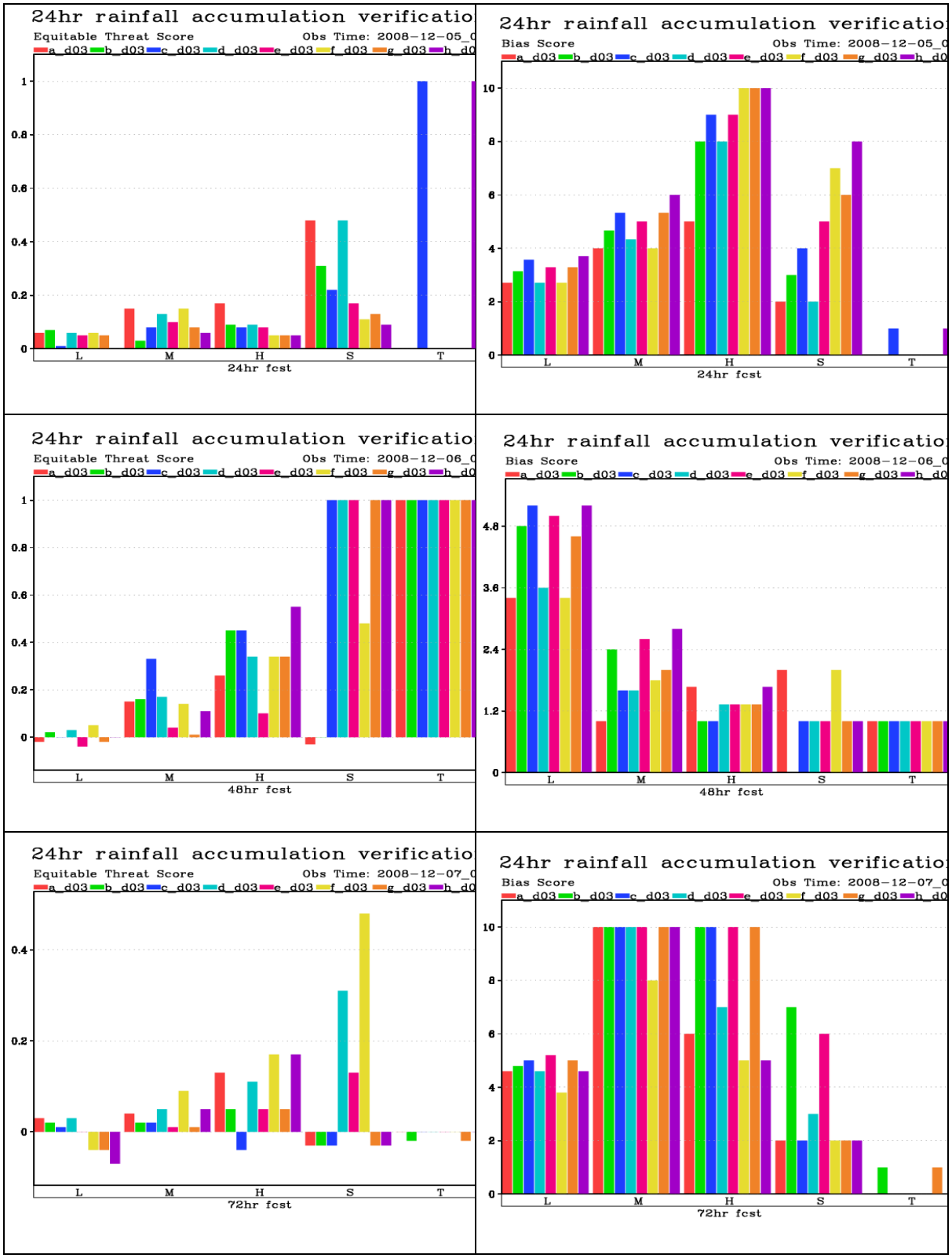

FIGURE 10B: ETS and Bias Scores for Case 2 over Peninsular Malaysia

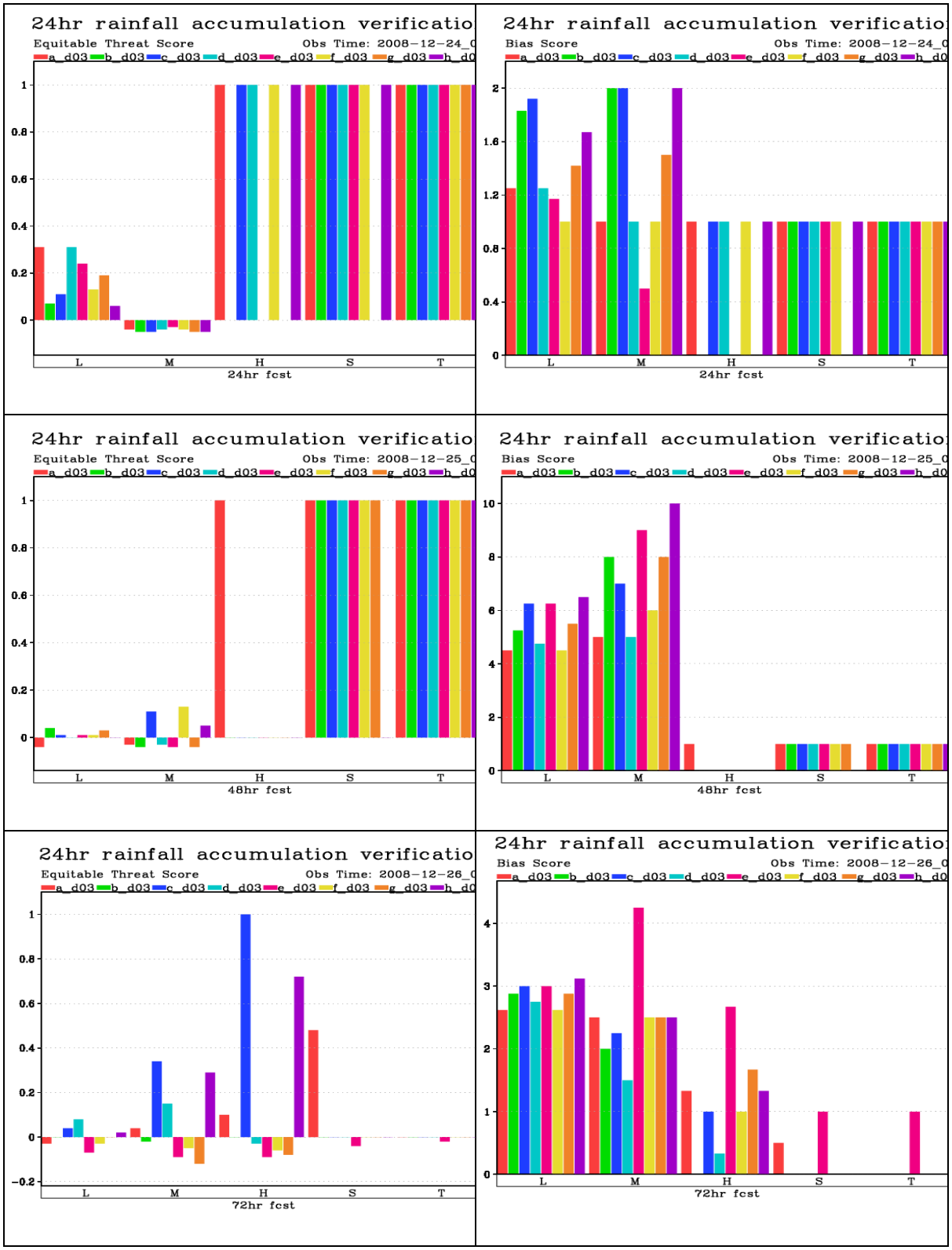

FIGURE 10C: ETS and Bias Scores for Case 3 over Peninsular Malaysia

6.0 Concluding Remarks

In tropics, the triggering mechanism for convection is always present. The convective available potential energy is always high and it is mostly the Convective inhibition energy which determines convection. However, the mechanism modulating rainfall during the northeast monsoon is primarily due to large scale convergence and synoptic scale forcing.

The behavior of the cumulus parameterization scheme (CPS) is tends to vary from the onset of the cold surge to the end of the surge episode. Based on the initial inference , the Tiedtke Scheme coupled with the BMJ Scheme seem toperform slightly better that the rest of the combinations. The sensitivity of nested runs to the cumulus parameterization used in their parent domain's run has been shown. This sensitivity increases with time and exerts influence on the location, timing, and intensity of the rain bands.

If we take a closer look at the Tiedtke Scheme, the entrainment for deep convection is made to depend on environmental moisture which helps the simulated tropical systems. The updated CAPE closure for deep convection relaxes CAPE generated in the planetary boundary layer which improves the diurnal precipitation over land. The convective adjustment time is no longer constant, but it depends on the vertical velocity averaged in the updraft and cloud depth.

7.0 Reference

Attada, R., Dasari, H. P., Kunchala, R. K., Langodan, S., Niranjan Kumar, K., Knio, O., & Hoteit, I. (2020). Evaluating Cumulus Parameterization Schemes for the Simulation of Arabian Peninsula Winter Rainfall, Journal of Hydrometeorology, 21(5), 1089-1114. Retrieved Jan 3, 2023

Xalxo, K.L., Mahala, B.K., Mohanty, P.K. et al. Performance assessment of WRF model radiation schemes in simulating the track and intensity of the super cyclonic storm “Amphan”. Nat Hazards 114, 1741–1762 (2022).

Huoqing Li 1,2,Hailiang Zhang 1, ,Ali Mamtimin 1, ,Shuiyong Fan 2 and Chenxiang Ju, 2020: A New Land-Use Dataset for the Weather Research and Forecasting (WRF) Model, Atmosphere 2020, 11(4), 350.

Fadila Jasmin Fakaruddin, Weng Sang Yip, Jeong Yik Diong, Ambun Dindang, Nursalleh K. Chang, Muhammad Helmi Abdullah, 2019: Occurrence of meridional and easterly surges and their impact on Malaysian rainfall during the northeast monsoon: a climatology study, RMetS.

Ooi See Hai, Azizan Abu Samah, Sheeba Nettukandy Chenoli, Kumarenthiran Subramaniam, and Muhammad Yunus Ahmad Marzuki, 2017: Extreme Rainstorms that Caused Devastating Flooding across the East Coast of Peninsular Malaysia during November and December 2014 , Weather and Forecasting.

Melina-Maria Zempila, Theodore M. Giannaros, Alkiviadis Bais, Dimitris Melas, Andreas Kazantzidis, Evaluation of WRF shortwave radiation parameterizations in predicting Global Horizontal Irradiance in Greece, Renewable Energy,Volume 86,2016,Pages 831-840,ISSN 0960-81

Grell, G. A., and S. R. Freitas, 2014: A scale and aerosol aware stochastic convective parameterization for weather and air quality modeling. Atmos. Chem. Phys., 14, 5233–5250

Almazroui, M., 2011: Calibration of TRMM rainfall climatology over Saudi Arabia during 1998–2009. Atmos. Res., 99, 400–414

Huffman, G. J., R. F. Adler, D. T. Bolvin, and E. J. Nelkin, 2010: The TRMM Multi-Satellite Precipitation Analysis (TMPA). Satellite Rainfall Applications for Surface Hydrology, F. Hossain and M. Gebremichael, Eds., Springer-Verlag, 3–22

Hong, S.-Y., and J.-O. J. Lim, 2006: The WRF Single-Moment 6-Class Microphysics scheme (WSM6). J. Korean Meteor. Soc., 42, 129–151.

Wilks, D., 2006: Statistical Methods in the Atmospheric Sciences: An Introduction. 2nd ed. Academic Press, 627 pp.

Arakawa, A., 2004: The cumulus parameterization problem: Past, present, and future. J. Climate, 17, 2493-2525.

Kain, J. S., 2004: The Kain-Fritsch convective parameterization: An update. J. Appl. Meteor., 43, 170-181. Kain, J. S., and J. M. Fritsch, 1990: A one dimensional entraining/detraining plume model and its application in convective parameterization. J. Atmos. Sci., 47, 2784-2802.

Grell, G. A., and D. Devenyi, 2002: A generalized approach to parameterizing convection combining ensemble and data assimilation techniques. Geophys. Res. Lett., 29, 1693-1696.

Morcrette, J.-J., Impact of the radiation-transfer scheme RRTM in the ECMWF forecasting system, ECMWF Newsletter No. 91, 2001

Iacono, M.J., E.J. Mlawer, S.A. Clough and J.-J. Morcrette: Impact of an improved longwave radiation model, RRTM. on the energy budget and thermodynamic properties of the NCAR community climate mode, CCM3. J. Geophys. Res., 105, 14873-14890, 2000

Mlawer, E.J., S.J. Taubman, P.D. Brown, M.J. Iacono and S.A. Clough: RRTM, a validated correlated-k model for the longwave. J. Geophys. Res., 102, 16,663-16,682, 1997

Janjic, Z. I., 1994: The step-mountain eta coordinate model: Further development of the convection, viscous sublayer, and turbulence closure schemes. Mon. Wea. Rev., 122, 927-945.

Betts, A. K., and M. J. Miller, 1993: The Betts Miller scheme. The Representation of Cumulus Convection in Numerical Models, Meteor. Monogr., No. 24, Amer. Meteor. Soc., 107-121.

Kain, J. S., and J. M. Fritsch, 1993: Convective parameterization for mesoscale models: The Kain-Fritsch scheme. The Representation of Cumulus Convection in Numerical Models,Meteor. Monogr., No. 24, Amer. Meteor. Soc., 165-170.

Betts, A. K., and M. J. Miller, 1986: A new convective adjustment scheme. Part II: Single column tests using GATE wave, BOMEX, ATEX and arctic air-mass data sets. Quart. J. Roy. Meteor. Soc., 112, 693–709

Arakawa, A., and W. H. Schubert, 1974: Interaction of a cumulus cloud ensemble with the large-scale environment, Part I. J. Atmos. Sci., 31, 674–701

Skamarock, W. C., J. B. Klemp, J. Dudhia, D. O. Gill, Z. Liu, J. Berner, W. Wang, J. G. Powers, M. G. Duda, D. M. Barker, and X.-Y. Huang, 2019: A Description of the Advanced Research WRF Version 4. NCAR Tech. Note NCAR/TN-556+STR, 145 pp.

MALAYSIA METEOROLOGICAL DEPARTMENT
JALAN SULTAN
46667 PETALING JAYA
SELANGOR DARUL EHSAN
Tel : 603-79678000
Fax : 603-79550964
www.met.gov.my

ISBN 978-967-2327-12-7